Journal of Materials Chemistry A

REVIEW

View Article Online
View Journal | View Issue

Cite this: J. Mater. Chem. A, 2017, 5, 11983

Perovskite oxides – a review on a versatile material class for solar-to-fuel conversion processes

Markus Kubicek, *[ab] Alexander H. Bork[ac] and Jennifer L. M. Rupp [ac]

Thermochemical water and carbon dioxide splitting with concentrated solar energy is a technology for converting renewable solar energy into liquid hydrocarbon fuels as an alternative to fossil fuels, which are dominating in today's energy mix. For the conversion reaction to be efficient, special redox materials are necessary to perform the necessary chemical reactions in a thermochemical cycle. Through this review we carefully examine perovskite oxides to design and optimize next generation solar-to-fuel conversion materials operating on thermochemical cycles. To date efforts have primarily been directed to binary oxides among which most prominently ceria was selected. Despite the promise, ceria has an unfavorable high reduction temperature and is restricted in its opportunities to manipulate through extrinsic doping the oxygen nonstoichiometry and thermodynamic properties for oxygen exchange towards H_2O and CO_2 splitting. In contrast, recent reports highlight new opportunities to use and alter perovskite oxides in terms of elemental composition over a wider range to affect reduction temperature, oxygen exchange characteristics needed in the catalytic reactions and fuel yield. To further foster perovskites for solar-to-fuel conversion, we review basic concepts such as the lattice structure and defect thermodynamics towards CO_2 and water splitting, discuss the role of oxygen vacancies and present strategies for an efficient search for new perovskite compositions. Summarizing, recent efforts on perovskite oxide compositions investigated are based on Fe, Mn, Co, or Cr with reported fuel yields of up to several hundred μmol per g per cycle in the literature. This article reviews the underlying principles, the latest advances and future prospects of perovskite oxides for solar-to-fuel technology.

Received 31st January 2017
Accepted 12th May 2017

DOI: 10.1039/c7ta00987a

rsc.li/materials-a

[a]Electrochemical Materials, ETH Zurich, Hönggerbergring 64 (HPP P 21), 8093 Zurich, Switzerland. E-mail: markus.kubicek@tuwien.ac.at

[b]Institute of Chemical Technology and Analytics, TU Wien, Getreidemarkt 9, 1060 Wien, Austria

[c]Electrochemical Materials, Massachusetts Institute of Technology, Cambridge, MA, 02139, USA

1. Introduction

Efficient utilization of solar energy is a major challenge of our time to satisfy the increasing energy demand of our civilization. Finding alternatives to replace the extensive usage of non-renewable fossil fuels and nuclear energy sources is the quest

Markus Kubicek is a postdoctoral scientist at Technische Universität Wien at the Institute of Chemical Technologies and Analytics, where he received his M.Sc and PhD in Chemistry in 2009 and 2013. From 2013 to 2015 he worked as postdoctoral scientist at ETH Zürich in the Department of Materials. He is working in the field of solid-state electrochemistry on mixed conducting materials for energy and memory applications. His current research focus is on perovskite oxides for solid oxide fuel cells, for solar-to-fuel conversion and as non-volatile resistive switching memories.

Alexander Hansen Bork receives his PhD degree in June 2017 in Materials Science and Engineering at ETH Zürich in Switzerland. Prior he graduated the M.Sc. Honors Program on Hydrogen and Fuel Cells at the Technical University of Denmark in 2013. Following his PhD he joins MIT as postdoc to pursue his research interest in the development of perovskite oxides through experiment and theory for solar thermochemical energy conversion.

of the 21st century to meet global energy demands, but also to reduce the greenhouse effect and environmental pollution hazards.[1–3] Nuclear energy sources are debatable in terms of safety, and there remains the general geographical dependency and non-equal distribution of all materials and fossil energy resources. Here, an attractive thought is to improve the geographical independence on politically critical elements for both the energy supply and its storage, and to capitalize in higher shares on solar energy to impact global safety, market and political stabilization.

Solar energy is abundant on earth with the earth receiving ~120 000 TW per year, which exceeds the annual energy consumption of ~15 TW by almost 4 orders of magnitude.[4–6] However it is intermittent and dilute with a maximum power at a sea level of about 1 kW m^{-2} and an average power of roughly 200 W m^{-2} depending on the effective geographic location.[4,7] Besides natural photosynthesis, several technologies exist to utilize solar energy. Photovoltaics are the most prominent example, where sunlight is converted into electrical energy, which is either used locally or delivered to the power grid. A challenge arises when it comes to storage of solar energy *e.g.* to buffer the intermittent supply of day–night and seasonal cycles or for buffering the alternating power grid usage. An electrical energy storage solution from photovoltaics would be batteries. Unfortunately, most of today's battery materials require in parts elements which are socio-economically critical[8,9] (*e.g.* cobalt) or not abundant (*e.g.* rare earth) and do not allow for a global and economically independent energy storage solution even with the best recycling efforts. Novel and alternative energy storage solutions are required to match the global availability of material structures and resources and transition towards geographically independent production and storage of renewable energy and fuels.

Three areas will directly benefit from renewable energy storage solutions as fuels, namely, the constant energy supply for stationary and industrial sector, buildings and transportation. Importantly, for transport or industrial processes often exclusively liquid fuels are demanded, for which today fossil fuels are almost entirely used. Hence it is necessary to develop processes for efficient conversion of solar energy to liquid fuels as a renewable alternative. Such processes are often categorized with the term "solar-to-fuel" and are typically based on photochemical or thermochemical reaction cycles. Similar to natural photosynthesis, H_2O and CO_2 are the low-chemical-energy starting compounds. They are then converted by solar energy to produce H_2 or CO or "syngas" being a mixture of both. The produced gas mixtures can then be chemically converted into liquid fuels (methanol, gasoline, kerosene, *etc.*) *via* Fischer–Tropsch synthesis to increase the energy density for storage and supply.[10–12] Different techniques to perform these energy conversions from H_2 or CO are described elsewhere, see ref. 7 and 10–18. We will focus on the primary techniques to produce H_2 and/or CO. Thermochemical cycles are an important solar-to-fuel technique. Here, the heat energy of concentrated sunlight is used to drive endothermic reactions of the cycle at high temperature while subsequent exothermic reactions are enabled after cooling at lower temperatures. Such thermochemical cycles are beneficial as the full solar spectrum can be utilized and there is a temporal separation for O_2 and H_2 production.[14,17,19–21] The resulting theoretical efficiency make thermochemical cycles a very promising energy technology. Annual conversion efficiencies over 20% can be reached as shown by the examples in Table 1 for a selection of different materials (*e.g.* iron, zinc or manganese oxide) and solar collector setups (*e.g.* dish or tower plant) based on data from Sandia National Laboratories.[22] It can be concluded, that theoretical solar-to-fuel conversion efficiencies exceed solar to hydrogen efficiency of photovoltaics combined with conventional electrolysis.[20,22]

Jennifer Rupp is the Thomas Lord Assistant Professor at the Department of Material Sciences and Engineering at the Massachusetts Institute of Technology (MIT) where she heads the Electrochemical Materials Laboratory. Since 2012, she holds two career awards at ETH Zurich being an ERC (SNSF) Starting Grant and SNSF professorship. Prior she was affiliated as senior scientist and postdoc to MIT, NIMS Tsukuba in Japan and ETH Zurich, where she received her PhD in 2006. Her research interests lay in developing alternative green and fair-trade energy materials and device operation schemes or suggesting novel neuromorphic computing architectures transferring data with low footprint. Here, ceramic-engineering from large scale processing to thin film structures and the design of the structure-charge and mass transport reactions is the key. Ethically she believes that material scientists and engineers can make important contributions defining next materials and device operation schemes to profit from renewables and transferring the opportunities to society, economy and politics.

2. Working principle of solar-to-fuel conversion

2.1 The thermochemical cycle

The conceptually most simple approach is to directly split H_2O (or CO_2) into H_2 and O_2 (CO and O_2) in concentrated sunlight at extremely high temperatures > 2000 K where the splitting reactions become thermodynamically more favorable. The gases are then separated and useable for fuel production at lower temperatures. Feasibility of this direct approach has been shown in solar-driven prototype plants for CO_2 splitting.[23] To avoid the extremely high temperatures, which are undesirable due to heat loss and material demands, metal oxides are commonly used to enable the splitting reaction at lower temperatures. In contrast to a catalyst in chemistry, which has to be present only in trace amounts, the fuel yield per cycle depends directly on the amount of the oxide in the reactor. In metal oxide based thermochemical cycles, the endothermic

Table 1 Efficiencies of solar thermochemical hydrogen production in different reaction cycles from Sandia National Laboratories for tower or dish solar concentrators[22]

Cycle name	Highest operation temperature	Solar plant type	Thermo-chemical efficiency	Optical efficiency	Receiver efficiency	Annual efficiency for H_2 production
Conventional electrolysis		Tower	30%	57%	83%	14%
Zinc oxide	1800 °C	Tower	45%	51%	72%	16.5%
Manganese oxide	1550 °C	Tower	50%	55%	78%	21%
Cadmium carbonate	1450 °C	Tower	50–70%	50%	67%	20%
Conventional electrolysis		Dish	26%	85%	86%	19%
Iron oxide	2100 °C	Dish	50%	74%	62%	23%
Zinc ferrite	1800 °C	Dish	52%	77%	62%	25%

reaction is the release of oxygen from the metal oxide at higher temperature. In the low temperature cycle oxygen from H_2O (or CO_2) is incorporated into the metal oxide again, thus producing H_2 (or CO). The materials in use, their thermodynamics and kinetics, as well as their chemical and mechanical stability are determining the characteristics of the optimal thermochemical cycle for solar-to-fuel conversion. For commercial implementation, cycle efficiency then has to be competitive compared to other materials and also to other technologies, for instance to photovoltaics and subsequent electrolysis.

Thermochemical production of syngas consists of a series of endothermic and exothermic reaction steps, which we detail in the following: in the first endothermic step, the metal oxide is reduced by solar thermal energy (eqn (1)) and in the second step, the reduced metal oxide is oxidized by either H_2O or CO_2 (eqn (2a) and (2b)). The process is exemplified in Fig. 1 for a perovskite (ABO_3) based solar-driven thermochemical redox cycle:

$$ABO_3 \leftrightarrow ABO_{3-\delta} + \frac{\delta}{2}O_2(g) \quad (1)$$

$$ABO_{3-\delta} + \delta H_2O \leftrightarrow ABO_3 + \delta H_2(g) \quad (2a)$$

$$ABO_{3-\delta} + \delta CO_2 \leftrightarrow ABO_3 + \delta CO(g) \quad (2b)$$

The Gibbs free energy change of the individual reaction steps depends on the perovskite composition, temperature and pressures. Here, Δg_{red} is the free energy change of reduction in eqn (1), and Δg_{gs} corresponds to the free energy change for the gas splitting reaction in eqn (2). The Gibbs free energy change of the total reaction, Δg_{gs}, must be negative for the reaction to be spontaneous or at least be close to zero to acquire a significant amount of products in chemical equilibrium. Consequently, the reduction reaction is typically carried out at low oxygen partial pressure and high temperature, whereas the gas splitting reaction is carried out at a comparably lower temperature $T_{ox} < T_{red}$. The Gibbs free energy change of water gas splitting is given by the free energy change associated with oxidizing the perovskite and water dissociation in the process.

$$\Delta g_{gs,H_2O} = \Delta g_O + \Delta g_{H_2O} \quad (3)$$

An analogous expression can be written for CO_2 splitting. Consequently, efficient catalyst materials must satisfy following the thermodynamic criteria:

- $\Delta g_{red}(pO_{2,red}, T_{red}) < 0$.
- $\Delta g_{oxd}(pO_{2,ox}, T_{ox}) < -\Delta g_{H_2O}(pO_{2,ox}, T_{ox})$.
- $\Delta g_{oxd}(pO_{2,ox}, T_{ox}) < -\Delta g_{CO_2}(pO_{2,ox}, T_{ox})$.

The thermodynamic requirements, reactor temperatures and $p(O_2)$ ranges for solar fuel production have been discussed in more detail in review articles by Scheffe and Steinfeld, Perkins and Weimer and Kodama[10,25,26] and also by Bilgen *et al.*, Kaneko *et al.* and Tamaura *et al.* for new material cycles.[27–29]

Feasibility of thermochemical cycles using metal oxides was already shown in the 1970s for iron oxide.[30] A number of metal oxides have been investigated since, the most promising results were reported using materials based on the oxides of iron, zinc and cerium. For the case of iron, the oxidation and reduction

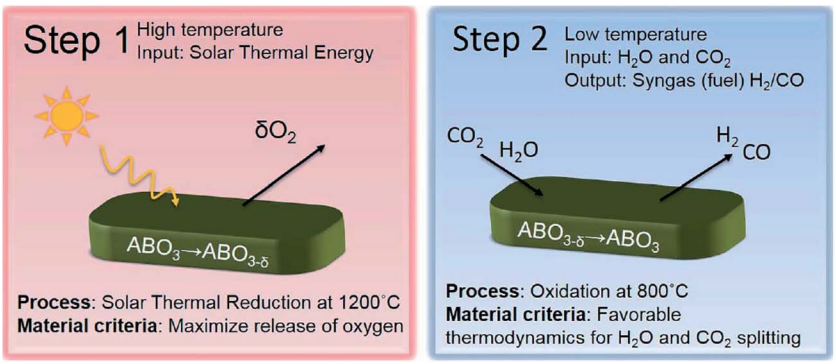

Fig. 1 Schematic of the 2-step water-splitting or CO_2-splitting reaction using a non-stoichiometric perovskite oxide.[24] In high-temperature step 1, the perovskite is reduced under oxygen evolution, in low temperature step 2 the perovskite is re-oxidized, thus producing H_2/CO.

reactions between Fe^{2+} and Fe^{3+} are typically used and in addition to the direct use of iron oxides (FeO, Fe_2O_3, and Fe_3O_4)[30–32] also Fe^{2+}/Fe^{3+} transitions in spinels were systematically studied.[29,33] For zinc oxide, the high temperature reduction of Zn^{2+} in ZnO to metallic zinc showed promising results[34,35] and besides basic research, the system was also studied up to pilot scale.[36,37] However, several downsides exist such as the temperature range, phase transitions and the reactivity of metal vapors. For those reasons, other metal oxides, which remain solid and in the same phase during the whole thermochemical cycle received increasing attention.

Cerium oxide fulfills these requirements as a reactor material, as both the oxidized and reduced form of $CeO_{2-\delta}$ have the same crystal structure. Literature is available for ceria-based materials on efficiency and doping,[38–45] structural design,[46,47] and different reactor types.[17,48,49] Recently, even the full solar to kerosene process has been successfully shown by the Steinfeld group using undoped ceria in a high temperature solar reactor to produce 700 liters of syngas which were converted by Fischer–Tropsch synthesis to a mixture of naphtha, gasoil and kerosene.[50] Till date, the high efficiency and high chemical and thermal stability of ceria and its solid solutions compared to other materials define the state-of-the-art for thermochemical fuel cycles and set a benchmark for new material developments in the field.

Perovskite oxides for thermochemical solar-to-fuel cycles have only been studied recently, but with fast-growing interest. The reason is that the perovskite structure is energetically very stable so that perovskite oxides are a very versatile material class being able to structurally accommodate a large variety of elements of the periodic table. By these characteristics opportunities exist to tune the catalytic, non-stoichiometry or photo- and electrochemical properties over a wider range when compared to binary oxides.[51–54] This versatility is also reflected by the many application areas of perovskite oxides being active components in batteries, fuel cells or photovoltaic electrode materials, non-metallic catalysts, dielectrics, multiferroics, resistive switches or sensing materials as summarized in the following review papers, see also Table 2.[51–55] Till date, first studies on solar-to-fuel conversion for perovskites were performed on manganite-based perovskite compositions.[56–66] However, also other compositions with different transition metals and combinations thereof showed promising results such as perovskite oxide solid solutions with the general structure ABO_3 including Co/Cr[24] or Fe/Co[67] on the B-site. The advantages of perovskites are clearly their flexibility, and therefore the possibility to tune their thermodynamic parameters and the immanent promise of finding an optimal material for high efficiency solar-to-fuel conversion. Also, the shift to lower operation temperatures is a benefit of most perovskite compositions simplifying requirements for solar-to-fuel reactors and their operation schemes. The requirements for an optimal perovskite material, however, are manifold: for example, perovskite oxides suffer often from either a lower entropy change compared to ceria which make the temperature cycles less efficient, or from large relative loads of H_2O/CO_2 being necessary at the reoxidation step.[68] Besides favorable thermodynamics, also defect chemistry, reaction kinetics, chemical stability as well as their thermal and mechanical stability need to be considered.

Table 2 Large variety of properties of different perovskite materials[53]

Compound	Property
$MgSiO_3$	Mantle mineral
$CaTiO_3$	Dielectric
$BaTiO_3$	Ferroelectric
$PbZr_{1-x}Ti_xO_3$	Piezoelectric
$Ba_{1-x}La_xTiO_3$	Semiconductor
$Y_{0.33}Ba_{0.66}CuO_{3-\delta}$	Superconductor
$LnCoO_{3-\delta}$	Mixed electronic ionic conductor
$SrCeO_3$	Proton conductor
$Li_{0.5-3x}La_{0.5+x}TiO_3$	Lithium ion conductor
$La_{1-x}Sr_xGaO_{3-\delta}$	Fast oxide ion conductor
$BaInO_{2.5}$	Fast oxide ion conductor
$KCaF_3$	Fast fluoride ion conductor
$NaxWO_3$	Electrochromic
$LaMnO_{3-\delta}$	Colossal magnetoresistance
$BaLiF_3$	Optical material

2.2 Solar concentrators and reactors

Solar reactors and concentrators are a vast research field summarized by the term Concentrated Solar Power (CSP) or Concentrated Solar Thermal (CST) technology. It is not only used for thermochemical solar-to-fuel cycles as in principle any endothermic reaction can be performed using CST. Within the scope of this paper on perovskite materials for solar-to-fuel conversion only a short overview on basic technical aspects of CST can be given. A setup for performing solar thermochemical cycles generally consists of two major parts. Firstly, in order to reach the high temperatures necessary to perform the reduction process of the oxide, a solar concentrator setup is necessary. Here, sunlight is concentrated into a reaction chamber, which is typically filled with the metal oxide being exposed to the reaction gases to perform the solar-driven redox reactions. Secondly, a mechanism is installed to the solar-concentrator, which allows changing between the low and high temperature regime and gas feeds for the operation points of the thermochemical cycles.

Several designs for solar concentrators have been presented, and examples used in commercial concentrated solar power plants are summarized in Fig. 2. The first two, parabolic troughs and linear Fresnel setups, are 2D concentrators, while dish/engine and central receiver setups are 3D concentrators. The higher solar concentration ratio C (defined as the mean solar radiative power flux over the focused area normalized to the direct normal incident solar radiation) can be achieved with 3D concentrators. Consequently, they allow for higher operation temperatures, which makes them better suited for thermochemical solar to fuel processes. Typically, C ranges from 200–3000 in existing 3D concentrator setups.[7] Excellent overviews on the topic are given by Yadav and Banerjee,[69] Said *et al.*,[70] and Romero and Steinfeld,[7] to which we refer for further details. It is to be noted that the reactor design is not independent of the

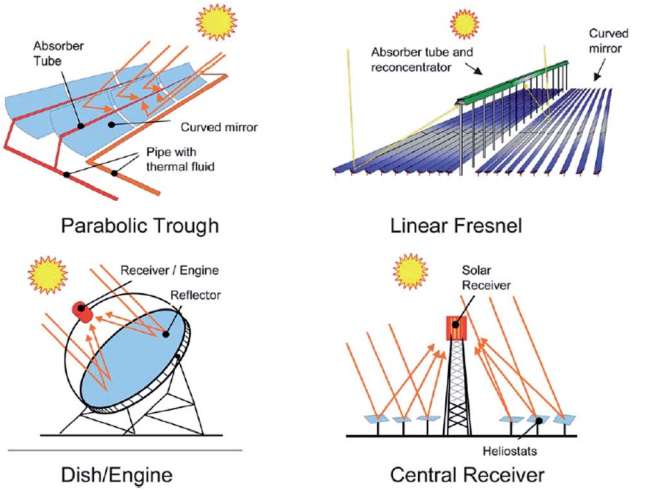

Fig. 2 Schematic of the four solar concentrating technologies currently applied at commercial plants: parabolic trough collectors, linear Fresnel reflector systems, dish-engine systems and power towers also known as central receiver systems. Reproduced from ref. 7 with permission from The Royal Society of Chemistry.

concentrator and the main challenges are good absorption of the solar energy, homogeneous heat distribution and good interaction with the gas phase allowing for fast and efficient chemical reactions. Further, thermal losses during the cycle need to be minimized. An efficient solar reactor allows continuous or quasi-continuous operation and heat recuperation to improve thermal efficiency. The former is either realized by having several batches in different operation points of the thermochemical cycle or by mass transfer of the oxidized and reduced oxide to enable the thermochemical cycle. Examples for a batch-type temporal cycle reactor and a continuous reactor concept are given in Fig. 3. Reactor types reported in the literature either as pilot plant or as concept include multi-tubular reactors,[71] fixed bed reactors,[72] fluidized bed reactors,[73,74] moving packed bed reactors,[75] counter-rotating ring reactors,[31] solar vortex reactors,[76–78] or reactors using liquid metal for efficient heat transfer.[79] Recent improvements in reactor design and cycle management have helped increase the total efficiency of the solar to fuel process to above 5%.[80]

For lab-scale experiments, *e.g.* for testing new material compositions or extracting thermodynamical parameters, commonly thermogravimetry (TG) based setups, small irradiation furnaces, or lab-size fluidized bed reactors are used for test purposes.[24,56–67]

3. Perovskite materials for solar-to-fuel conversion

3.1 Structure and physical properties of perovskites

To understand the opportunities of perovskites for solar-to-fuel conversion we introduce the structural concept behind those materials and highlight implications of solid solution doping on their oxygen exchange, catalysis and splitting needed for thermochemical conversion. Ideal perovskite structures adopt a cubic symmetry and crystallize in the space group $Pm\bar{3}m$ with the chemical formula ABX_3 shown in a structural schematic in Fig. 4. The large majority of perovskites with technical application are oxides. Here A is the larger cation with 12-fold coordination, B is the smaller cation with octahedral, 6-fold coordination and X refers to an oxygen ion O^{2-}. Also several closely related layered structures or defective structures exist which are also referred to as perovskite-type materials in the literature. Examples are the Ruddlesden–Popper-series $A_{n+1}B_nX_{3n+1}$ (ref. 81) or double perovskite structures $A_2B_2X_{5+\delta}$.[82,83] However, also non-oxide perovskites exist such as halide perovskites (X = halide) which have attracted much interest recently as materials for photovoltaics[84,85] or anti-perovskites where A and B are anions and X are cations.[86,87] Returning to the more common oxide perovskites, a break from the ideal cubic $Pm\bar{3}m$ symmetry is regularly observed depending on the chemistry and elements selected for the ABO_3 structures.† The large variety of electronic, ionic or magnetic properties that can be achieved with perovskites is a consequence of the large number of chemical elements and different cations that can successfully be incorporated on the A- or B-sites in the crystal lattice. Several examples for properties of different perovskite materials collected by Stolen *et al.*[53] are shown in Table 2.

This structural flexibility to stabilize several different distorted lattices and the connection to the ionic radii of the involved ions were already the subject of investigations back in the 1920s. Goldschmidt introduced a tolerance factor t based on the ionic radii of the A and B site cations,[88] which is still used as a figure of merit to characterize perovskites.[54] The idea behind the Goldschmidt tolerance factor is based on the correlation between structural geometry and the ionic radii of the cations. The tolerance factor t is calculated according to eqn (4) using the radii r_N of the ions for the general perovskite formula ABX_3.

$$t = \frac{r_A + r_X}{\sqrt{2}(r_B + r_X)} \quad (4)$$

For an ideal cubic perovskite where the ions are touching the tolerance factor is $t = 1$. In contrast, deviations of t to higher or lower values than $t = 1$ demonstrate an increased tendency for structural distortions in the lattice. Distortions can lead to a lowering of the symmetry from cubic to orthorhombic, rhombohedral, tetragonal, monoclinic or triclinic, with the first two being the most common for perovskites.[51,52,55] The most relevant properties of a perovskite used for thermochemical cycles are the reactivity for oxygen exchange and H_2O/CO_2 splitting. A suitable perovskite requires a large range of oxygen non-stoichiometry, a well-fitting enthalpy of formation for oxide defects (usually oxygen vacancies) and mobile electronic carriers to enable the exchange reaction at the surface. In the next section the defect chemistry of perovskites will be discussed in more detail with regards to an efficient solar-to-fuel material.

† Note that slightly distorted structures (*e.g.* in atomic distances and/or angles) are nonetheless in the literature often referred to as "perovskite materials" or "pseudocubic" perovskites.

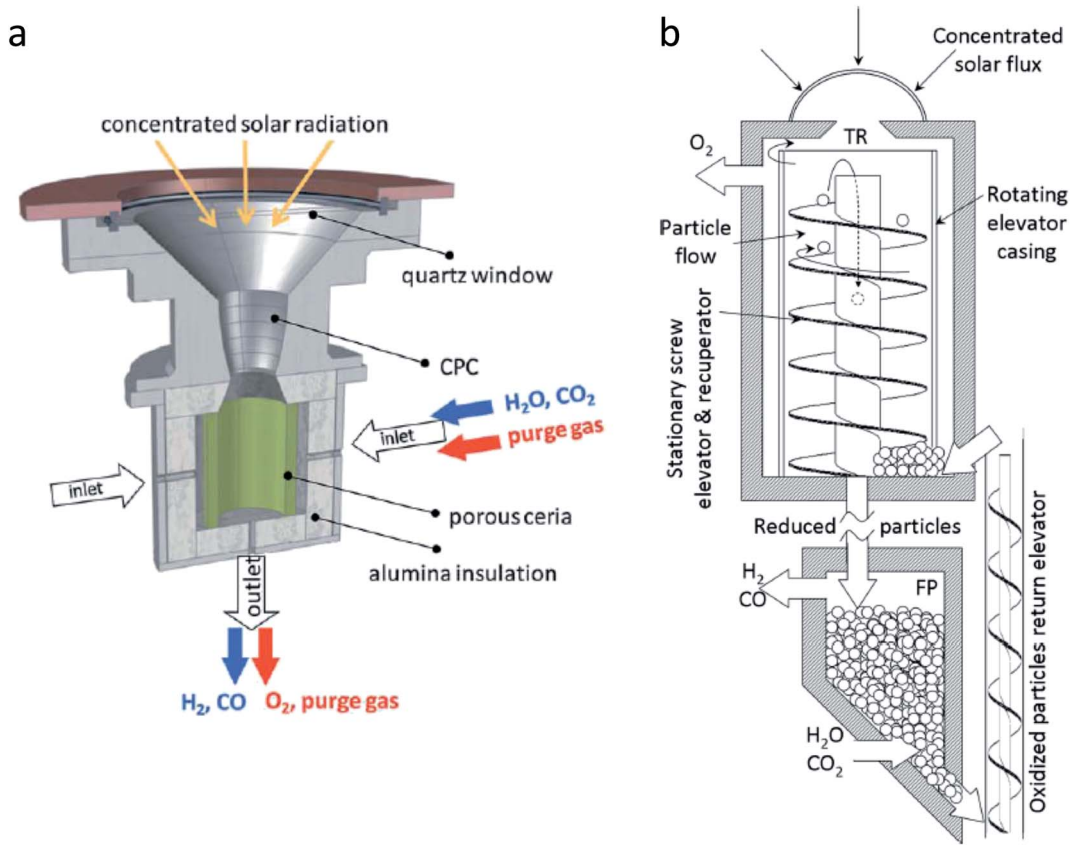

Fig. 3 Schematics of two different solar reactor concepts: (a) solid state reactor using porous ceria for temporally separated H_2O or CO_2 redox reactions from Steinfeld group at ETH Zurich. From W. C. Chueh, C. Falter, M. Abbott, D. Scipio, P. Furler, S. M. Haile and A. Steinfeld, *Science*, 2010, **330**, 1797–1801. Reprinted with permission from AAAS. (b) Moving particle bed reactor described by Ermanoski *et al.*[75] with a spatially separated thermal reduction chamber (TR) and fuel production chamber (FP) and continuous operation. Reprinted with permission from I. Ermanoski, N. P. Siegel and E. B. Stechel, *Journal of Solar Energy Engineering*, 2013, **135**, 031002. Copyright ASME.

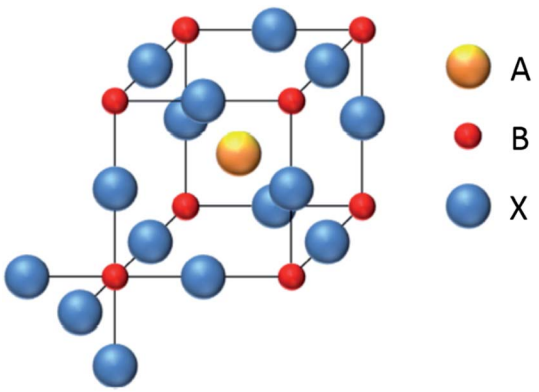

Fig. 4 The ideal cubic $Pm\bar{3}m$ structure of an ABX_3 perovskite. For oxides, X is to the oxide ion O^{2-}, A is a large 12-fold coordinated cation, and B is a small 6-fold (octahedral) coordinated cation.

3.2 Mechanism of oxygen exchange and defect chemistry in perovskites

In contrast to materials which decompose or change their phase during thermochemical redox cycles for solar-to-fuel conversion such as zinc oxide, perovskites are supposed to retain a single phase under reducing and oxidizing conditions for long-term durability. In solar-to-fuel conversion the fuel yield and detailed reaction kinetics are largely driven by the oxygen incorporation and release of the perovskite material. Here, lattice defects in the perovskite control the equilibrium thermodynamics and the kinetics of the thermochemical redox-cycles also, which we consider through the following in their defect type and characteristics for the process: point defects are the most important defect type for perovskites in solar-to-fuel conversion, as they react in their thermodynamic equilibrium to external drivers such as temperature or oxygen partial pressure $p(O_2)$. Three types of point defects‡ can exist in perovskite oxides: *electronic defects, oxygen ionic defects and cationic defects*.

(i) *Electronic defects* are either electrons e^- or electron holes $h^\bullet$ in the lattice structure. Both types are present in certain concentrations for undoped perovskites at room temperature, or are intentionally introduced to these by extrinsic doping which is frequently done to produce either n-type (donor-doped)

‡ Note that higher dimensional extended defects such as dislocations, *etc.* are typically not in thermodynamic equilibrium. They can be important for kinetics[89,90,142–148] but in contrast to point defects they cannot be utilized for thermochemical cycles. For further background the reader is referred to ref. 91.

or p-type (acceptor-doped) conducting perovskites. For solar-to-fuel conversion, electronic charge carriers are important to enable charge transfer at the surface reaction (either oxygen incorporation or release) and as fast charge carriers for ambipolar diffusion which is necessary to distribute oxygen vacancies in the whole reactor material.

(ii) For *oxygen ionic defects*, typically only one type of defect exists in ABO_3 perovskite oxides, namely *oxygen vacancies*. These are p-type defects like electron holes but of double charge. Oxygen interstitials (the n-type analogue) are energetically much more unfavorable in cubic or pseudo-cubic perovskite oxides.[52] The main reason is that the perovskite structure is densely packed and creating extra space for interstitial ions is closely linked with large energy penalties. For example, (La,Sr)$MnO_{3+\delta}$ (LSM), which is sometimes (formally incorrectly) reported in the literature contains cation vacancies rather than oxygen interstitials and should accordingly be named $(La,Sr)_{1-x}Mn_{1-y}O_3$.[92,93] The fact that in perovskites interstitials are more unfavorable than vacancies is not a general rule for all oxides and is closely related to the respective crystal structure. For perovskite solar-to-fuel reactor materials, oxygen vacancies have a very central role. They are important to enable oxidation and reduction of the material while retaining the phase. The change in oxygen vacancy concentration between the oxidation conditions and the reduction conditions has a direct impact on the fuel yield per cycle. Further, both the kinetics of the surface exchange of oxygen as well as the diffusion in the material are influenced by oxygen vacancies. They will be discussed in more detail in Section 3.2.1.

(iii) For similar reasons as for oxygen defects, *cationic defects* also typically only exist as vacancies and not as interstitials. Computational studies on $LaMnO_3$,[94] $LaFeO_3$,[95] and $LaGaO_3$ (ref. 96) show that the Schottky disorder resulting in vacancies is way more favorable than the Frenkel disorder leading to cation interstitials.[94–96] Besides (La,Sr)MnO_3 under oxidizing conditions which forms cation vacancies as already mentioned above, there exist several compositions which can accommodate relatively large numbers of cation vacancies. Vacancies on the A-site are more common and calculations show that those are also energetically favorable to B-site vacancies.[94] An example for perovskites stabilizing a large number of A-site cation defects are La-doped titanates such as $Sr_{1-1.5x}La_xTiO_3$, where A-deficient compositions in the whole stoichiometry range $0 \leq x \leq 2/3$ were investigated.[97,98] For the perovskite solar-to-fuel processes reported in the literature, cation defects are usually of minor or no importance.

3.2.1 The role of oxygen vacancies. The single most important defects for solar-to-fuel application are oxygen vacancies, which are necessary in order to incorporate and release oxygen. The difference of oxygen vacancies in the perovskite under oxidizing and reducing conditions determine the maximum convertible mass in each thermochemical cycle. Oxygen non-stoichiometry limits are given by the stability of the crystal structure and phase transformations. As oxygen interstitials are unfavorable, in a perovskite $ABO_{3-\delta}$ the highest oxidized state is therefore typically reached at $\delta = 0$ or ABO_3. The most reduced state in perovskites is reached at or close to $\delta = 0.5$ or $ABO_{2.5}$ for most compositions. There, a pseudo-cubic perovskite often converts into $A_2B_2O_5$ phases such as brownmillerite *e.g.* $LaSrCo_2O_5$ or $Sr_2Fe_2O_5$.[99] But also several other $A_2B_2O_5$ phases are known[53] such as the different structures taken by $Sr_2Mn_2O_5$ (ref. 100) by $La_2Ni_2O_5$ (ref. 101) and by $La_{8-x}Sr_xCu_8O_{20}$.[102] However, phase decomposition at $\delta = 0.5$ is not a general rule for perovskites. Some materials exist which decompose into different metal oxides already at lower non-stoichiometry. There are, on the other hand, also few examples of cubic or pseudo-cubic perovskites which retain their phase even beyond $\delta = 0.5$. A special case is $Ba_{1-x}Sr_xCo_{1-y}Fe_yO_{3-\delta}$ (BSCF).[103,104] Here, non-stoichiometry higher than $\delta = 0.8$ has been measured by thermogravimetry and neutron scattering[105] as shown in Fig. 5. In BSCF even at high oxygen pressures and moderate temperatures very high oxygen vacancy concentrations are present, *e.g.* $\delta = 0.65$ (ref. 105) at 600 °C in 1 bar O_2. However, together with the high non-stoichiometry, for BSCF also a low chemical stability and phase instabilities are reported.[106,107]

The example of BSCF shows that for certain perovskite oxides it is possible to retain phase stability even with more than 1 out of 4 oxygen sites being unoccupied. A possible shift of oxygen non-stoichiometry in that order is very promising for perovskites in solar-to-fuel thermochemical cycles. But even utilizing "only" a sizeable part of the oxygen vacancies in a more typical non-stoichiometry region of $0 \leq \delta \leq 0.5$ or 16.7% of total oxygen sites for a perovskite structure of $ABO_{3-\delta}$ would already be well beyond the state-of-the art for solar-to-fuel applications. For example, using ceria as the benchmark, only about 2% of the oxygen sites in ceria can be actively used *e.g.* for splitting of H_2O or CO_2 (ref. 38). The highest non-stoichiometry of ceria in a thermochemical cycle is reached at reduction, typically at

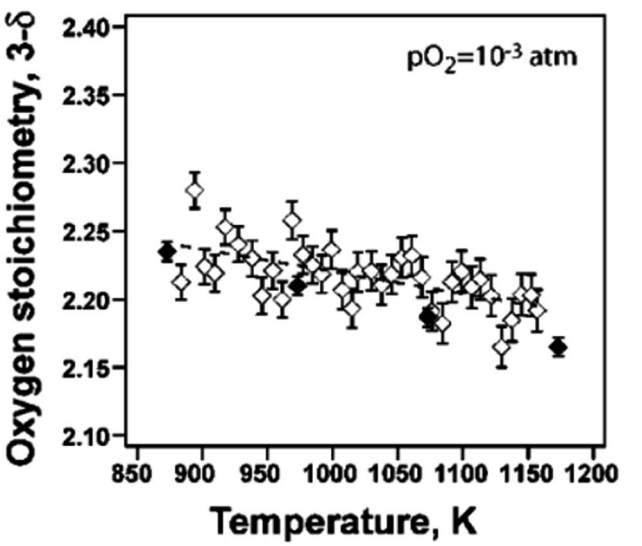

Fig. 5 Extremely high oxygen non-stoichiometry δ found in the $Ba_{0.5}Sr_{0.5}Co_{0.8}Fe_{0.2}O_{3-\delta}$ perovskite. Adapted with permission from S. McIntosh, J. F. Vente, W. G. Haije, D. H. A. Blank and H. J. M. Bouwmeester, *Chem. Mater.*, 2006, **18**, 2187–2193. Copyright 2006 American Chemical Society.

1500 °C, and there in thermodynamic equilibrium, only about 3% of all oxygen sites are unoccupied at $p(O_2) = 10^{-5}$ mbar.[38,108]

3.2.2 Mechanisms of oxygen exchange. Various perovskites have been suggested for solar-to-fuel conversion which we want to examine in light of their oxygen exchange mechanisms. The studies reported in the literature using perovskites for thermochemical cycles used predominantly highly p-doped perovskites based on either manganese,[56–66] chromium,[24] cobalt,[24] or iron[67] on the B-site of the perovskite lattice. The p-type doping is compensated by positively charged defects – a mixture of electron holes and oxygen vacancies changing in their concentrations upon oxidation/reduction. Those oxides are then typically used as extrinsic materials for the whole temperature range of the solar-thermochemical cycle. Extrinsic means that the total p-type defect level is set by the doping and in good approximation doesn't change with temperature. The change in oxygen stoichiometry of the material upon filling or releasing of oxygen vacancies is then used for H_2O or CO_2 splitting in the oxidation reaction.

All third-row transition metals mentioned above, namely, Mn, Cr, Co, and Fe have in common the fact that they can exist in oxidation state 3+ and that they form stable perovskites together with La^{3+}, *e.g.* $LaMnO_3$. Introducing p-type doping is then regularly done by replacing some of the La^{3+} lattice sited by Sr^{2+},[24,56–67] but also other cations such as Ca^{2+} or Ba^{2+} can be used, see Table 3. The reasons are the fixed oxidation state of both La^{3+} and Sr^{2+} and their similar ionic radii[109] which also fit well to the size of the transition metal and oxide ion for a perovskite crystal structure. The Goldschmidt tolerance-factor *e.g.* for $La_{0.8}Sr_{0.2}MnO_3$ is $t \sim 0.99$ based on Shannon's ionic radii.[109] Values close to $t = 1$ are geometrically and also structurally favorable for perovskites, see previous chapter 3.2.

We will now have a closer look at the defect chemistry using $(La,Sr)MnO_{3-\delta}$ as an example which is one of the most investigated perovskite composition for solar-to-fuel conversion, see Table 3. The basic composition is lanthanum manganite $LaMnO_3$; here both lanthanum and manganese have the oxidation state 3+ and the perovskite is a small band gap oxide.[110] Replacing La^{3+} by Sr^{2+} and allowing no oxygen exchange, we see that according to eqn (5) this chemically results in a mixed valence Mn^{3+} and Mn^{4+} on the B-site, where "Mn^{4+} on a Mn^{3+} site" and "electron hole" are two formally different descriptions of the same property. The material is now a good electronic conductor with a metal to insulator transition.[111,112]

$$La^{3+}Mn^{3+}O_3 \xrightarrow{+xSr^{2+}-xLa^{3+}} La_{1-x}{}^{3+}Sr_x{}^{2+}Mn^{(1-x)3+,(x)4+}O_3 \quad (5)$$

Allowing now oxygen exchange following the chemical potential equilibrium with the atmosphere according to eqn (6), a defect equilibrium forms between electron holes and oxygen vacancies.

$$La_{1-x}{}^{3+}Sr_x{}^{2+}Mn^{(1-x)3+,(x)4+}O_3 \leftrightarrow La_{1-x}{}^{3+}Sr_x{}^{2+}Mn^{(1-x+2\delta)3+,(x-2\delta)4+}O_{3-\delta} + \frac{\delta}{2}O_2 \quad (6)$$

The total number of the p-type defects in the composition of LSM is now fixed by the amount of Sr-doping (x). It is distributed among electron holes and vacancies and their relation is formulated in eqn (7), in Kröger–Vink notation.[113]

$$x = h^{\cdot} + 2V_O^{\cdot\cdot} \quad (7)$$

We can now simplify the whole oxygen exchange reaction (eqn (6)) of a p-type extrinsic perovskite oxide to eqn (8). At high temperature and low $p(O_2)$ the equilibrium shifts to the right and *vice versa* at low temperature and high $p(O_2)$.

$$O_O^{\times} + 2h^{\cdot} \leftrightarrow V_O^{\cdot\cdot} + \frac{1}{2}O_2 \quad (8)$$

We can conclude that high levels of p-type extrinsic doping are suitable for perovskite oxides to control the thermochemical cycles by their defect chemistry. At low temperatures (and/or high oxygen partial pressures) their doping is compensated primarily by electron vacancies, while at high temperature oxygen is released and a major part of the electron holes are converted into oxygen vacancies as defects. The difference to ceria which is often used as a benchmark for solar-to-fuel conversion is that in pure ceria oxygen vacancies are generated intrinsically, which means without doping. There, oxygen vacancies are generated at high temperatures *via* the release of oxygen. Hence, two electrons per oxygen atom released remain in the solid, which makes reduced ceria an electron conductor.

3.3 Thermodynamics of oxygen release of perovskites in relation to the thermochemical splitting cycle

The thermodynamics of the oxygen release reaction of perovskite materials is a useful descriptor to identify suitable compositions for thermochemical gas splitting.[114–116] Fit candidates must have favorable oxidation thermodynamics for H_2O and CO_2 splitting and subsequent reduction to higher non-stoichiometry. Several perovskite oxides can accommodate high non-stoichiometry at moderate temperatures and oxygen partial pressure based on their defect chemistry, but only a few of those are able to re-oxidize in the presence of water and carbon dioxide.

3.3.1 Thermodynamic properties of perovskites obtained by thermogravimetric measurements. In order to compare the suitability of the respective compositions and in search of new perovskite materials, one can benefit from the wide literature available on the thermodynamics of the oxygen release in perovskites obtained by thermogravimetric analysis. One can profit not only from the literature of the solar-to-fuel field, but also from other fields investigating mixed electronic ionic conducting perovskites *e.g.* as electrodes for solid oxide fuel cells. In Fig. 6, we present data of the Gibbs free energy change of reduction, Δg_O, as a function of temperature for various perovskites at a representative oxygen non-stoichiometry after thermal reduction of $\delta = 0.1$. In addition, we plot the Gibbs free energy change of the water (blue line) and carbon dioxide splitting reaction (red line). The physical meaning of being

above the blue (red) line is that splitting of H_2O (CO_2) is thermodynamically favorable. We compare perovskite ABO_3-compositions with partial substitution of lanthanum by strontium and/or calcium on the A-site and various transition metals on the B-site to embody the perovskite materials investigated in the solar-to-fuel field.[24,56–67] The only materials, depicted in this plot, that are not tested in the solar-to-fuel technology are $La_{0.9}Ca_{0.1}CrO_{3-\delta}$, $La_{0.7}Sr_{0.3}Cr_{3-\delta}$ and $LaCr_{0.9}Ni_{0.1}O_{3-\delta}$. They are included to illustrate the large variations in the thermodynamic properties of perovskites.

Based on the data in Fig. 6, we can summarize the following trends of favorability of gas splitting: firstly, it is clear that the composition $La_{0.6}Sr_{0.4}MnO_{3-\delta}$ is below the red and blue lines for the measured temperature range reflecting unfavorable thermodynamics for gas splitting. Secondly, the doped lanthanum chromates, *i.e.* $La_{0.9}Ca_{0.1}CrO_{3-\delta}$, $La_{0.7}Sr_{0.3}CrO_{3-\delta}$, $LaCr_{0.9}Ni_{0.1}O_{3-\delta}$, generally have favorable thermodynamics for oxidation in the presence of water and/or carbon dioxide. Thirdly, it can be expected that solid solutions of $La_{0.7}Sr_{0.3}Co_{1-y}Fe_yO_{3-\delta}$ and $LaMnO_3$ with Ca/Sr A-site and Al B-site doping have thermodynamic properties between those of their constituents and therefore have unfavorable thermodynamics for gas splitting. Despite having unfavorable thermodynamics for gas splitting, solid solutions of *e.g.* Sr-doped $LaMnO_3$ have shown considerable fuel production yields of up to 300 μmol per g per cycle in the literature.[56,62,125] The main reason for this difference is that these experiments were carried out with a large excess of H_2O and CO_2, in contrast to the representation above displayed for one mole of reactant gas per one mole of perovskite. With an excess reactant concentration, it is possible to shift the chemical equilibrium towards the production of H_2 and/or CO. Here it is important to consider that utilizing excess gas reactants leads to an energy penalty in the overall thermochemical efficiency. For determination of the materials potential for efficient thermochemical gas splitting, we refer the reader to the following ref. 121, 126 and 127. In order to exploit the versatility of the perovskite material class towards favorable thermodynamics of the water splitting reaction one can mix cations at the very top with materials at the bottom of this plot. For example, it is beneficial to introduce Cr-substitution on the B-site due to its high value of Δg_O together with for example Co or Fe. This will create a perovskite with the ability to tune, by a large degree, the thermodynamic properties as exemplified by the results for the composition $La_{0.6}Sr_{0.4}Cr_{1-x}Co_xO_{3-\delta}$.[24]

Most data shown in Fig. 6 were derived from thermochemical studies which were originally measured for temperature ranges of 900–1200 K applicable for perovskites in *e.g.* solid oxide fuel cells. Considering that the solar-to-fuel operation range is between 900–1800 K, one should be careful when extrapolating thermodynamic properties and the actual behavior of the materials over such a wide temperature range. However, in summary, an Ellingham-type diagram such as this representation gives substantial first indications on where to make and study potential perovskites for solar-to-fuel conversion.

3.3.2 Thermodynamics of the oxygen release reaction in perovskites obtained by computational analysis. As an alternative to model non-ideal solution behavior and thermodynamics of the oxygen release reaction over a wide temperature range of complex perovskite oxides one can turn to the CALPHAD (CALculation of PHAse Diagrams) approach.[128–131] There are several advantages of applying the comprehensive CALPHAD approach: firstly, the description of thermodynamics and defect chemistry takes all available data from a wide range of experiments, covering a wider temperature range, taken into consideration upon extrapolation. Secondly, the approach enables a description of multicomponent systems on a physicochemical base. The latter is particular useful for evaluation of perovskites, since the ABO_3 structure can host an immense number of different elements on both A- and B-sites, which enables assessment of new materials.[131] One drawback of the comprehensive CALPHAD approach, is that establishment of the predictive multi-component CALPHAD database with applicability for defect chemistry simulations is demanding because it requires experimental input beyond determination of oxygen contents in the perovskite phase. Nevertheless, many important subsystems that govern perovskite thermodynamics are available,[132–135] and understanding of first-principles analysis of oxide phase thermodynamics has become deeper,[130,136] and thermodynamic data of oxide phases for CALPHAD assessments can be realized. See Bork *et al.*[131] for details on application of the CALPHAD approach for solar to fuel conversion on the perovskite system $La_{1-x}Sr_xMnO_3$.

Other computational approaches to describe and predict the oxygen vacancy formation energetics in perovskites include density functional theory (DFT).[136–139] For example, Emery *et al.*[136] demonstrated a high-throughput computational screening of perovskites for thermochemical water splitting by DFT. In this work, a large data set of 5329 perovskites, with a single A-site cation and a single B-site cation, were studied both in terms of compound stability and oxygen vacancy formation. The authors were able narrow down the possible compositions and identify 139 potential perovskite candidates with favorable thermodynamics for water splitting. Density functional theory has also proven useful in describing perovskite oxides with more than one cation on the A- and B-site. Deml and co-authors studied the perovskite systems $La_{1-x}Sr_xMO_{3-\delta}$ (M = Cr, Mn, Fe, Co)[137] and the more complex oxide $La_{1-x}Sr_xMn_{1-y}Al_yO_{3-\delta}$ with two different metals on both cationic sites.[138] The findings in these studies help guide the design of future perovskite materials and further the understanding of effects of doping and the nature of the oxygen vacancy formation.

In summary, density functional theory calculations are very useful to screen the vast number of possible perovskite compositions and understanding the nature of the defect formation. Subsequently, it may be complimented by thermogravimetric measurements or CALPHAD models to capture the relation between oxygen nonstoichiometry and temperature as well as the enthalpy and entropy of oxygen vacancy formation as function nonstoichiometry, which are

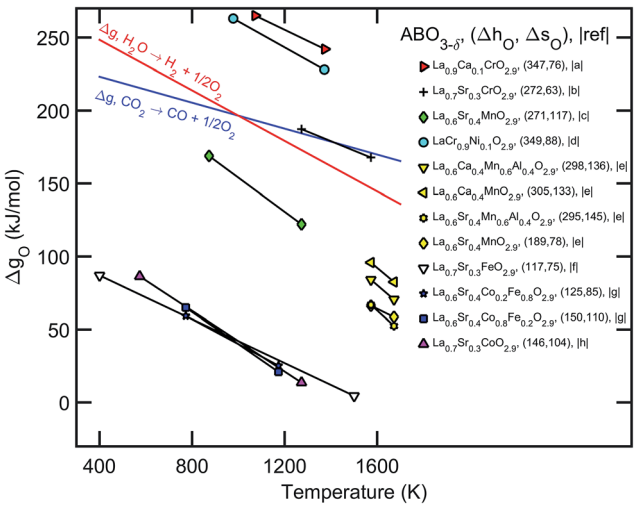

Fig. 6 Reaction partial molar Gibbs free energy change, Δg_O, for the defect forming reaction $O_O^{\times} + 2Me_{Me}^{\cdot} \rightleftharpoons 1/2O_2(g) + V_O^{\cdot\cdot} + Me_{Me}^{\times}$, at an oxygen non-stoichiometry of $\delta = 0.1$, plotted as a function of temperature. The symbols are identical for the same composition, *e.g.* a diamond is used for $La_{1-x}Sr_xMnO_3$, and the same color is used for material thermodynamics coming from one reference. The enthalpy, Δh_O (kJ mol^{-1}), and entropy, Δs_O (J mol^{-1} K^{-1}), of oxidation are included in parenthesis at the given non-stoichiometry. The following perovskites are considered; (a) $La_{0.9}Ca_{0.1}Cr_{3-\delta}$, Onuma *et al.*,[117] (b) $La_{0.7}Sr_{0.3}CrO_{3-\delta}$, Mizusaki *et al.*,[118] (c) $La_{0.6}Sr_{0.4}MnO_{3-\delta}$, Mizusaki *et al.*,[119] (d) $LaCr_{0.9}Ni_{0.1}O_{3-\delta}$, Oishi *et al.*,[120] (e) $La_{1-x}Me_xMn_{1-y}Al_yO_{3-\delta}$, M = Ca, Sr, $x = 0$, 0.2, 0.3, 0.4, $y = 0$, 0.4, Cooper *et al.*,[121] (f) $La_{1-x}Sr_xFeO_{3-\delta}$, $x = 0.1$, 0.2, 0.3 Mizusaki *et al.*,[122] (g) $La_{1-x}Sr_xFe_{1-y}Co_yO_{3-\delta}$, $y = 0.2$, 0.8, Kuhn *et al.*,[123] and (h) $La_{1-x}Sr_xCoO_{3-\delta}$, $x = 0.1$, 0.2, 0.3, Mizusaki *et al.*[124]

crucial for determination of the solar to fuel conversion performance.

3.4 Kinetics of perovskites in solar-to-fuel conversion processes

The thermochemical process, which was so far only described in its thermodynamic equilibrium states is for all practical purposes depending on kinetic parameters such as surface oxygen exchange rates or diffusion constant or the reactor material, reactor related heating/cooling or gas exchange rates, *etc.* One must be aware that even if the sum reaction for solar-to-fuel conversion is thermodynamically favorable, this does not necessarily mean that the reaction will run fast enough for useful conversion rates. We can split the areas of interest for kinetics into chemical and reactor-based parts which we assess individually. The perovskite|gas surface as the place where the chemical reactions happen is addressed first. Here the H_2O or CO_2 molecules are converted into H_2 or CO upon incorporating oxygen into the perovskite. Oxygen then has to be distributed in the perovskite bulk, a process governed by ambipolar diffusion, a diffusion of both negative and positive charge carriers to retain charge neutrality. Upon oxygen release the reaction direction is reversed and both, diffusion and surface exchange kinetics are again determining the reaction characteristics as shown in Fig. 7.

3.4.1 Chemical oxide reduction and re-oxidation kinetics.

Both surface exchange reactions *on* and diffusion *in* different perovskite oxides have been subject to intense research activities in the last years. Here, besides studies directly on solar-to-fuel, one can also profit from the research area of solid oxide fuel cells and solid oxide electrolysis cells (SOECs) working with very similar materials. The H_2O or CO_2 splitting reaction is directly comparable to the SOEC cathode reaction described in detail in several review-articles.[140–142] What needs to be considered, however, is that in contrast to fuel or electrolysis cells, no electrical potential difference is generated or desired in the oxygen exchange for solar-to-fuel conversion. Diffusion processes are ambipolar and driven only by a chemically induced gradient (by changing T and $p(O_2)$ in the two thermochemical reaction steps). The kinetics of oxygen release and oxygen non-stoichiometry of perovskites is of high interest for SOFC cathode materials and also there, several excellent overview articles exist.[140,143,144]

The chemical surface exchange coefficient, describes the kinetics of the surface reaction at thermochemical cycles. Mass relaxation[145] and conductivity relaxation[106,145–148] are important experimental tools to gather kinetic information on surface exchange and diffusion. In both cases, a small abrupt change of the oxygen partial pressure is performed, and the time dependence of the reaction of the sample is investigated. For mass relaxation, the mass loss (or increase) upon oxygen release (incorporation) is monitored. In the latter method, the conductivity change due to defect chemical changes is measured, see eqn (8). Upon oxygen incorporation, electron holes are produced (electrons consumed) and therefore the electronic conductivity increases for p-type oxides (decreases for n-type oxides). From the time dependence and/or geometrical changes of the sample, the chemical surface exchange coefficient (k_{chem}) and the chemical diffusion coefficient (D_{chem}) can be determined. Several perovskite oxides have been investigated, among them $(La,Ba,Sr)(Co,Fe)O_{3-\delta}$,[145,149] $(La,Sr)FeO_{3-\delta}$,[146,147] and $(La,Sr)CoO_{3-\delta}$.[148] In special experimental setups also by incorporating ^{18}O tracer, chemical diffusion profiles can be created and visualized *e.g.* by Secondary Ion Mass Spectrometry.[150] However, the chemical diffusion coefficient may not be confused with tracer or vacancy diffusion coefficients. For a detailed overview and differentiation, see ref. 151. Comparing the absolute values of k_{chem} and D_{chem} we typically find values in the order of 10^{-5} to 10^{-3} cm s^{-1} for k_{chem} and 10^{-7} to 10^{-6} cm^2 s^{-1} for D_{chem} at 600–800 °C for cobalt and iron perovskites.[145–149] The activation energy is positive which means that the kinetics at the temperatures of the reduction step are typically high enough to allow fast oxygen exchange, especially at high temperatures of >800–1500 °C regularly used in solar-to-fuel cycles. By reversing the argument, we also find that the oxidation temperature cannot be decreased to much lower temperatures. Here, the ionic transport processes would become very slow, and even though the driving force for the water splitting reaction may still increase, the conversion rates would drop towards zero. This sets a lower limit from a chemical point of view for decreasing the re-oxidation temperature of

a solar-to-fuel cycle using a metal oxide. Only few studies directly dedicated to the reaction kinetics in solar-to-fuel cycles exist and particularly so on perovskites. Yang, Haile *et al.*, observed that the hydrogen evolution kinetics in $La_{1-x}Sr_x$-$MnO_{3-\delta}$ at 800 °C depends strongly on the strontium content x. Higher strontium contents showed significantly slower kinetics, even though the total yield per cycle increased with increasing levels of strontium doping to the perovskite, see Fig. 8. For any new oxide composition studying the chemical exchange kinetics in important to get insight into a material dependent lower temperature boundary which is given by a minimum conversion rate necessary for efficient operation.

3.4.2 Physical and reactor-based influences on kinetics of a thermochemical cycle. During a thermochemical cycle, a reactor must be able to increase and decrease the temperature and change the $p(O_2)$ by either pumping or purging *e.g.* with N_2. An optimal reactor would ideally absorb the incident radiation throughout the whole cycle and provide a homogeneous distribution of $p(O_2)$ and temperature in the reaction zone and minimize heat loss to the outside. A real reactor will always differ from its ideal counterpart, which will have an impact on kinetics and efficiency. The consequences from incomplete absorption or heat losses are immediately clear, but also inhomogeneity hampers the reactor performance. For a simple solar reactor in a cavity (to reduce heat loss) that is filled with oxide and illuminated from one side, all heat and mass exchange will necessarily happen *via* the oxide surface. This will naturally lead to gradients at the different operation points in a cycle.[152,153] Temperature gradients from the illuminated to the non-illuminated side and chemical gradients from the gas inlets to the gas outlets are observed. Both of these gradients can lead to sluggish operation as the conversion reactions will only happen in a reaction front with the correct temperature and $p(O_2)$ which may travel slowly through the oxide. As a consequence, either the full redox potential of the oxide cannot be utilized, or a long cycle time has to be chosen which means more solar energy is used to produce the same amount of fuel. Both effects hamper conversion efficiency.

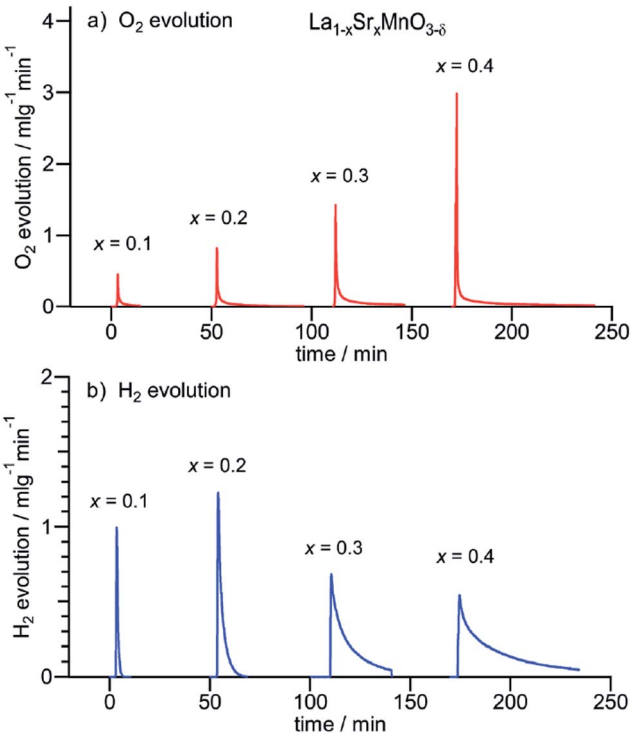

Fig. 8 Reaction kinetics of thermochemical water splitting using the $La_{1-x}Sr_xMnO_{3-\delta}$ perovskite. The O_2 evolution reaction at 1400 °C is fast for all investigated compositions $x = 0.1$–0.4. The H_2 evolution reaction at 800 °C becomes unfavorably slow for high Sr contents, even though the total fuel yield per cycle increases. Reproduced from ref. 56 with permission from the Royal Society of Chemistry.

Several strategies exist to simultaneously approach the challenges. For monolithic structures, porous media enhance the homogeneity *via* fast gas diffusion and enhanced surface. However, a limit is obvious, as by making structures more porous, more oxide material is removed from the reactor. The producible fuel per cycle depends directly on the amount of oxide in the reactor. Closed porosity is therefore especially

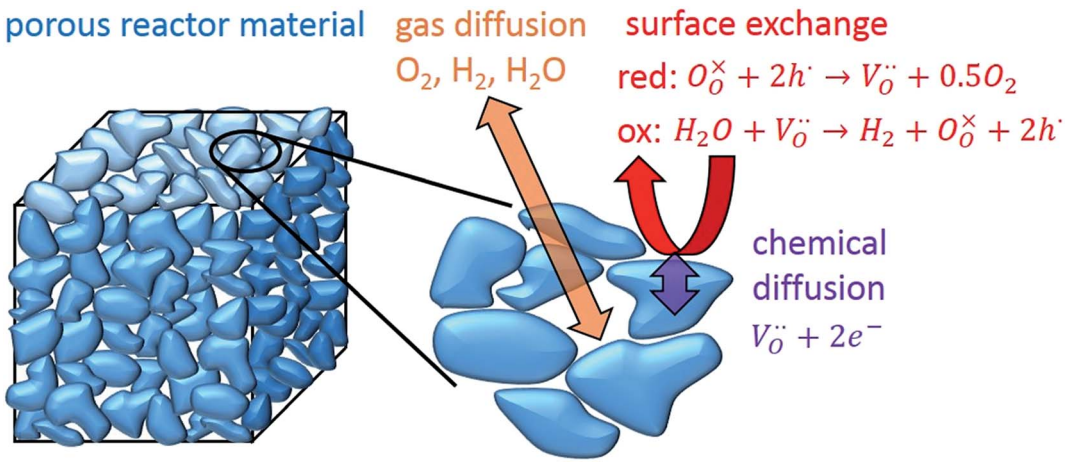

Fig. 7 Graphical overview of the possible kinetic bottlenecks limiting the conversion reaction in solar-to-fuel thermochemical cycles in a porous material: gas diffusion through pores, the redox-reactions at the surface and chemical diffusion into grains are shown.

undesired. Reticulated porous structures with two different pore sizes were shown to be a good compromise.[46,154,155] Two examples of different porous structures for use in solar reactors are shown in Fig. 9 based on ceria and zirconia-iron oxide. Another realization of good homogeneity and large surface area are bed reactors in which flowing powder in contact with the reaction gas will lead to homogeneous reaction conditions.[156–160] Also spatial separation of the radiation absorption step from the reaction chamber and transfer of heat *via* a heat transfer fluid has been suggested.[79]

3.5 Oxidation state of cations – spectroscopic methods

From the previous chapters it becomes clear that in order to design and suggest new optimized materials, we need to understand the different elemental constituents of perovskites and the changes which occur under different temperatures and $p(O_2)$ values. In particular for compositions containing several elements that can change their oxidation state it is important to know what element changes under which external influence. Several spectroscopic and diffraction-based methods are in use. X-ray absorption spectroscopy (XAS), X-ray photoelectron spectroscopy (XPS) and Raman spectroscopy will be discussed in more detail. Here, especially high pressure cells offer the possibility to perform synchrotron-based characterization of the materials not only at high vacuum conditions, but *in situ* at the high temperatures and pressures comparable to operating conditions. Here we will concentrate on Cr, Mn, Fe, and Co-based perovskites, which seem especially promising for solar-to-fuel conversion.

With X-ray absorption techniques, often the charge states or charge ordering are probed. A major question is, how exactly electron holes are distributed among the elements of the perovskites. A study on p-type doped manganites shows that the simple model of Mn^{3+} and Mn^{4+}, which was used to explain defect chemistry is found to be more complicated in reality. No real charge ordering is present, rather the charge is distributed between the Mn ions which are consequently in an oxidation state between 3+ and 4+.[161] However, still two different types of Mn ions do exist in the mixture, which differ more in their geometrical environment rather than in their charge.[161] Doping studies of manganite perovskite with other transition metals on the structural B-site show that Cr, Co and Ni all prefer lower oxidation states than manganese.[162,163] Introduction of those elements increase the oxidation state of Mn in p-type manganites. However, no ordering in pairs such as Co^{2+}/Mn^{4+} and Co^{3+}/Mn^{3+} but rather a homogeneous distribution of defects and charges is observed.[163] Also by doping of lower valent main-group elements such as Mg on a Mn site, Mn^{3+} in $LaMnO_3$ can be forced into Mn^{4+}.[164] Several studies also investigated the whole non-stoichiometry region from brownmillerite $ABO_{2.5}$ to cubic perovskite ABO_3 (ref. 165 and 166) and the associated changes in cation chemistry. For $SrCoO_{3-\delta}$, in addition with neutron scattering, several intermediate non-stoichiometries with defect ordering were observed.[165] Very similar defect associates were observed for $SrFeO_{3-\delta}$.[166]

Another important spectroscopy technique is X-ray Photoelectron Spectroscopy. Besides classical measurements in a high vacuum environment, again *in situ* measurements at elevated temperatures and partial pressures are of special significance. Here, near surface chemical information for several oxygen deficient perovskite oxides has been investigated mainly for application as a SOFC compound. $La_{0.75}Sr_{0.25}Cr_{0.5}Mn_{0.5}O_{3-\delta}$ showed surface coverage with Sr affecting the cation oxidation states at elevated temperatures which could be affected by applying an electric bias.[167] Similarly, $(La,Sr)CoO_{3-\delta}$ and $(La,Sr)_2CoO_{4-\delta}$ show Sr-rich surfaces that also affect the active sites for oxygen dissociation and incorporation.[168] For $(La,Sr)FeO_{3-\delta}$ reversible formation of Fe^0 at the surface was observed under water splitting conditions[169] based on *in situ* XPS investigations. Such ex-solutions or segregations on the

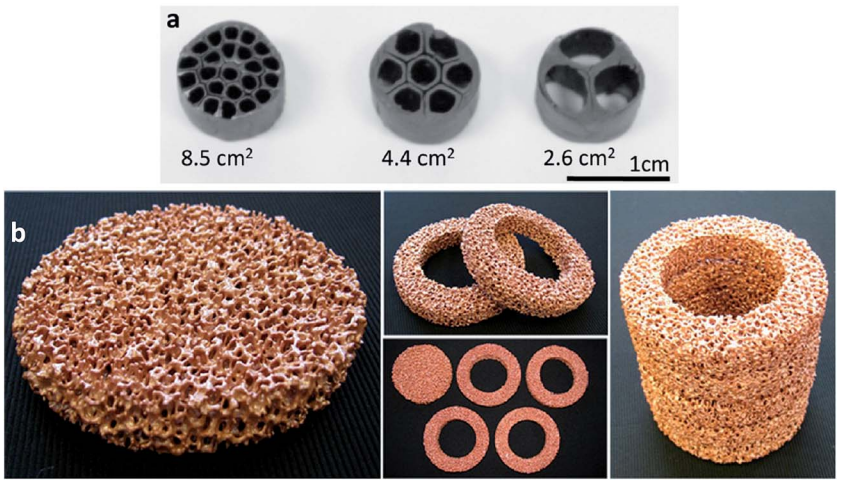

Fig. 9 Porous structures optimized for use in solar reactors. (a) Honeycomb structures with different pore sizes made from zirconia-iron oxide composites. Reprinted with permission from L. S. Walker, J. E. Miller, G. E. Hilmas, L. R. Evans and E. L. Corral, *Energy & Fuels*, 2012, **26**, 712–721. Copyright 2012 American Chemical Society. (b) Reticulated porous ceria ceramics with dual porosity. Reprinted with permission from P. Furler, J. Scheffe, M. Gorbar, L. Moes, U. Vogt and A. Steinfeld, *Energy and Fuels*, 2012, **26**, 7051–7059. Copyright 2012 American Chemical Society.

surface have detrimental influence on the redox kinetics and are one reason for the large differences in catalytic activity of different perovskite oxides.

Raman spectroscopy is a powerful tool to evaluate the defect structure by measurement of the changes in the near-order oxygen anionic–cationic bonds. Several researchers have studied the near-order crystal structure of lanthanum manganite perovskite systems by Raman spectroscopy, which was motivated by the perovskite's *Giant Magnetoresistivity*.[170–173] Additional studies have provided important information on the structure of doped La(Sr,Ca)MnO_3 systems[174,175] and a few studies on perovskites with the general formula $LaMeO_3$ (Me = Mn, Co, Fe).[176,177] Despite the potential of Raman spectroscopy for solar-to-fuel, a limited amount of studies employs it directly in this field. It was utilized to confirm structural changes in the ceria fluorite structure due to different oxygen contents.[178] The changes were detected by a shift in the Raman F_{2g} main peak at 465 cm^{-1} down to 464.5 cm^{-1} when the nonstoichiometry was changed from $\delta = 0$ to $\delta = 0.253$. The approach has been used directly on perovskites for solar-to-fuel, to determine the presence of trace amounts of secondary phase $SrCrO_4$ in the doped solid solutions $La_{0.6}Sr_{0.4}Cr_{1-x}Co_xO_{3-\delta}$. The presence of this phase was characterized by a high intensity peak observed at 870 cm^{-1} for the oxidized samples. In fact, it was found that this secondary phase could be removed by reduction at a temperature of 1200 °C. Overall, Raman spectroscopy is useful for detection of adverse secondary phases in perovskites but most importantly for examination of the structural changes as a function of the oxygen content, which is crucial for the fuel production capacity of solar-to-fuel materials.

4. Yield and thermochemical efficiency of solar-to-fuel thermochemical cycles based on perovskite materials

For perovskites, several studies on the performance of the thermochemical cycle for different materials are available in the literature. A direct comparison of the compositions by just one figure of merit is not possible due to the different temperature cycles, cycle times, gas partial pressures, fuel loads used in the individual studies. The parameter that is most often used in the literature to serve as a comparison to other materials is the fuel yield in μmol fuel per gram oxide employed in the thermochemical cycle. An overview of experimentally measured fuel yields is given in Table 3. Values of up to 757 μmol per g per cycle are reported, for reference, the fuel yield for CO for undoped ceria was shown to be about 169 μmol per g per cycle for an exemplary thermal reduction at 1500 °C and oxidation by CO_2 at 1000 °C.[24] The high fuel yields found by several groups displayed in Table 3 of perovskites demonstrate the viability of the perovskite compositions for production of H_2 and CO. Most investigated are perovskites containing manganese together with mixtures of La, Y, Sr, Ba, or Ca as shown in the following Table 3. Reduction temperatures are in the range 1000–1400 °C and oxidation temperatures in the range 800–1100 °C. In particular reducing the high reduction temperature compared to the usual 1500 °C with ceria is a major aim to achieve with new materials such as perovskites.

The majority of these studies were carried out under an inert flow *i.e.* low $p(O_2)$ and high flows of H_2O and/or CO_2 in combination with thermogravimetry and mass spectrometry, as well as floating bed reactors, or solar furnaces (lab-scale up to prototype-scale) to study the solar-to-fuel conversion characteristics.[24,56,57,61,62,64,65,67] Note that using excess reactant gas (*e.g.* steam) shifts the equilibrium of reaction eqn (2) towards higher fuel production, but unreacted educts lead to an overall energy penalty resulting in a lower thermochemical efficiency.[56,126,127] Overall, the fuel yields give a nice overview on what materials are promising; they cannot be used to predict competitiveness of the whole thermochemical cycle.

Often the thermodynamic efficiency of a solar-to-fuel process is used as a better guideline for possible commercial realization. The conversion efficiency η_{conv} of a thermochemical fuel generated is typically calculated as the enthalpy of the produced fuel ΔH_{fuel} divided by the heat input Q_{input}.

$$\eta_{conv} = \frac{\Delta H_{fuel}}{Q_{input}} \tag{9}$$

Siegel *et al.* discuss a 20% annual average solar-to-fuel efficiency for a competitive and successful commercial implementation.[20] Besides the thermodynamic equilibria for reduction of the oxide and oxidation by water/CO_2 splitting, also the chemical and thermal efficiency play a role. Here, materials that can exchange a large amount of oxygen during the cycle per volume or mass are desired. For thermal efficiency, a small change of the temperature between the oxidation and reduction step is beneficial. In the literature, several excellent calculations of equilibrium fuel yield and thermochemical efficiency exist.[116,126,127,179–181] Exemplarily, Scheffe *et al.*[126] calculated the thermochemical efficiency of the perovskite $La_{1-x}Sr_xMnO_{3-\delta}$ and compared that to the benchmark material, ceria. The equilibrium hydrogen fuel yields are calculated by solving the following eqn (10) iteratively,

$$\Delta g_O(\delta = \delta_i - n_{H_2}) = RT \ln\left(\frac{n_{H_2O}K_w}{n_{H_2}}\right) \tag{10}$$

where δ_i represents the oxygen non-stoichiometry at reduction, n_{H_2} is the equilibrium fuel yield, n_{H_2O} is water concentration, K_w is the equilibrium constant for water dissociation, and Δg_O is the partial molar free energy of oxidation. The study showed that the strontium doped lanthanum perovskites had larger fuel yields, but the solar thermochemical efficiency was higher for ceria under most relevant conditions.[126] Experimental data for efficiency calculations for different materials in the literature are most commonly based on data acquired by thermogravimetry, and often the data does not cover the entire technological relevant temperature range.[56,116,126,127,182] Clearly, the mentioned studies provide valuable information on the relative performance, one can anticipate discrepancies upon extrapolation of a single literature source to temperatures where measurements do not exist. As an alternative, CALPHAD (Calculation of Phase

Table 3 Fuel yields of perovskite oxides in H_2 or CO producing solar-to-fuel thermochemical cycles

Composition	Gas/fuel	Temperature range/°C	Fuel yield μmol per g per cycle	Ref.
$La_{0.9}Sr_{0.1}MnO_{3-\delta}$	H_2O/H_2	800–1400	10	56
$La_{0.8}Sr_{0.2}MnO_{3-\delta}$	H_2O/H_2	800–1400	33	56
$La_{0.7}Sr_{0.3}MnO_{3-\delta}$	H_2O/H_2	800–1400	65	56
$La_{0.6}Sr_{0.4}MnO_{3-\delta}$	H_2O/H_2	800–1400	102	56
$La_{0.65}Sr_{0.35}MnO_{3-\delta}$	CO_2/CO	1050–1400	198	57
$La_{0.5}Sr_{0.5}MnO_{3-\delta}$	CO_2/CO	1050–1400	215	57
$La_{0.35}Sr_{0.65}MnO_{3-\delta}$	CO_2/CO	1050–1400	151	57
$La_{0.2}Sr_{0.8}MnO_{3-\delta}$	CO_2/CO	1050–1400	117	57
$La_{0.5}Sr_{0.5}MnO_{3-\delta}$	CO_2/CO	1100–1400	325	62
$La_{0.65}Sr_{0.35}MnO_{3-\delta}$	H_2O/H_2	1050–1400	113	67
$La_{0.5}Sr_{0.5}MnO_{3-\delta}$	H_2O/H_2	1000–1400	160	67
$La_{0.5}Sr_{0.5}MnO_{3-\delta}$	H_2O/H_2	900–1400	133	67
$Y_{0.5}Sr_{0.5}MnO_{3-\delta}$	CO_2/CO	900–1400	757	61
$Y_{0.5}Sr_{0.5}MnO_{3-\delta}$	CO_2/CO	900–1300	624	61
$Y_{0.5}Sr_{0.5}MnO_{3-\delta}$	CO_2/CO	900–1200	418	61
$Y_{0.5}Sr_{0.5}MnO_{3-\delta}$	CO_2/CO	1050–1400	105	65
$Y_{0.5}Ca_{0.5}MnO_{3-\delta}$	CO_2/CO	1100–1400	671	61
$La_{0.5}Ca_{0.5}MnO_{3-\delta}$	CO_2/CO	1050–1400	168	65
$La_{0.5}Ca_{0.5}MnO_{3-\delta}$	CO_2/CO	1100–1400	525	62
$La_{0.65}Ca_{0.35}MnO_{3-\delta}$	CO_2/CO	1050–1400	188	65
$La_{0.65}Ba_{0.35}MnO_{3-\delta}$	CO_2/CO	1050–1400	159	65
$La_{0.5}Ba_{0.5}MnO_{3-\delta}$	CO_2/CO	1050–1400	149	65
$La_{0.6}Sr_{0.4}Mn_{0.6}Al_{0.4}O_{3-\delta}$	H_2O/H_2	1000–1350	307	64
$La_{0.4}Sr_{0.6}Mn_{0.6}Al_{0.4}O_{3-\delta}$	H_2O/H_2	1000–1350	277	64
$La_{0.6}Sr_{0.4}Mn_{0.4}Al_{0.6}O_{3-\delta}$	H_2O/H_2	1000–1350	220	64
$La_{0.6}Sr_{0.4}Mn_{0.6}Al_{0.4}O_{3-\delta}$	CO_2/CO	1000–1350	294	64
$La_{0.4}Sr_{0.6}Mn_{0.6}Al_{0.4}O_{3-\delta}$	CO_2/CO	1000–1350	286	64
$La_{0.6}Sr_{0.4}Mn_{0.4}Al_{0.6}O_{3-\delta}$	CO_2/CO	1000–1350	247	64
$La_{0.5}Sr_{0.5}Mn_{0.75}Al_{0.25}O_{3-\delta}$	CO_2/CO	1050–1400	186	65
$La_{0.6}Sr_{0.4}Mn_{0.6}Al_{0.4}O_{3-\delta}$	CO_2/CO	1050–1400	187	65
$La_{0.6}Sr_{0.4}Mn_{0.4}Al_{0.6}O_{3-\delta}$	CO_2/CO	1050–1400	180	65
$La_{0.5}Sr_{0.5}Mn_{0.85}Mg_{0.15}O_{3-\delta}$	CO_2/CO	1050–1400	183	65
$La_{0.6}Sr_{0.4}Mn_{0.83}Mg_{0.17}O_{3-\delta}$	CO_2/CO	1050–1400	207	65
$LaMn_{2/3}Mg_{1/3}O_{3-\delta}$	CO_2/CO	1050–1400	55	65
$La_{0.6}Sr_{0.4}Cr_{0.95}Co_{0.05}O_{3-\delta}$	CO_2/CO	800–1200	14	24
$La_{0.6}Sr_{0.4}Cr_{0.9}Co_{0.1}O_{3-\delta}$	CO_2/CO	800–1200	56	24
$La_{0.6}Sr_{0.4}Cr_{0.8}Co_{0.2}O_{3-\delta}$	CO_2/CO	800–1200	157	24
$La_{0.6}Sr_{0.4}Cr_{0.5}Co_{0.5}O_{3-\delta}$	CO_2/CO	800–1200	51	24
$La_{0.6}Sr_{0.4}Cr_{0.8}Co_{0.2}O_{3-\delta}$	H_2O/H_2	800–1200	50	24
$Ba_{0.5}Sr_{0.5}Co_{0.8}Fe_{0.2}O_{3-\delta}$	H_2O/H_2	800–1000	83	67
$La_{0.6}Sr_{0.4}Co_{0.8}Fe_{0.2}O_{3-\delta}$	H_2O/H_2	800–1200	51	67
$La_{0.6}Sr_{0.4}CoO_{3-\delta}$	H_2O/H_2	800–1300	107	67
$CeO_{2-\delta}$	CO_2/CO	1000–1500	169	22

Diagrams) data on defect chemistry can be used as input data to calculate equilibrium fuel yields and efficiency as recently demonstrated.[131,180]

Overall, the transfer of efficiencies extracted from lab experiments to a final industrial scale solar-to-fuel process are difficult. Jarrett *et al.* point out that efficiency calculations in the literature are often difficult to compare, as parameters such as the energy required to preheat unreacted species or vacuum pump efficiency are not considered uniformly.[183]

5. Conclusion

Thermochemical solar-to-fuel redox cycles are a promising energy technology which is renewable and gives perspective to profit more efficiently on intermittent energy production and to store solar light directly as a synthetic liquid fuel for buffer or usage. Optimal conversion catalysts, which are often called oxygen storage materials, are still to be developed. Here, perovskite oxides offer several exceptional features that encouraged research and development of this materials class towards solar-to-fuel conversion. The perovskite structure is very stable and is able to accommodate a huge concentration of oxygen vacancies, which can allow highly productive redox cycles and high fuel conversion yields without phase changes. On the other side, the ability of perovskite oxides to accommodate different chemical elements allows innumerable combinations of elements in stable solid solutions leaving a lot of space for improving existing materials. This flexibility is used

in first studies to tune the thermodynamic properties to fit the needs of a specific thermochemical cycle. Several mostly acceptor-doped perovskite compositions have been studied, among them manganites, ferrites, cobaltates, chromates or aluminates. The biggest advantages of perovskites compared to ceria is that a lower reactor temperature is sufficient for reduction, and the larger possible change of nonstoichiometry. Two aspects for perovskites which often still require improvement are their chemical stability and their inherent low enthalpies compared to ceria which hamper thermal efficiency and make larger temperature sweeps necessary. Further progress can be expected in the next years with both materials screening studies as well as computational techniques to predict promising new materials compositions. Besides the thermodynamic properties, also mechanical and thermal stability, chemical reactivity and reaction kinetics require favorable characteristics. These complex requirements are the challenges for materials and reactor design to exploit the potential of >20% efficiency with thermochemical cycles which surpasses existing solar fuel technologies such as coupled photovoltaics and electrolysis. Besides the acceptor-doped cubic perovskites which dominate today's research efforts, perovskite-related materials still offer a large variety of structures which have so far not been systematically tested such as layered structures, structures accommodating oxygen interstitials and many others, wherein highly efficient solar-to-fuel reactor materials might be found.

Acknowledgements

The financial support by ETH, grant number ETH-05 13-1, is gratefully acknowledged. JR thanks the Thomas Lord Foundation for support of her MIT professorship. Also, MITEI program and company Eni at MIT are gratefully acknowledged.

References

1 IPCC, *Climate Change 2013: The Physical Science Basis. Contribution of Working Group I to the Fifth Assessment Report of the Intergovernmental Panel on Climate Change*, Cambridge University Press, Cambridge, United Kingdom and New York, NY, USA, 2013.
2 *IPCC Special Report on Emissions Scenarios*, ed. N. Nakicenovic and R. Swart, Cambridge University Press, The Edinburgh Building Shaftesbury Road, Cambridge England, 2000.
3 OPEC, Annual Statistical Bulletin 2015, http://www.opec.org/opec_web/en/publications/202.htm.
4 R. E. Blankenship, D. M. Tiede, J. Barber, G. W. Brudvig, G. Fleming, M. Ghirardi, M. R. Gunner, W. Junge, D. M. Kramer, A. Melis, T. A. Moore, C. C. Moser, D. G. Nocera, A. J. Nozik, D. R. Ort, W. W. Parson, R. C. Prince and R. T. Sayre, *Science*, 2011, **332**, 805–809.
5 N. S. Lewis and D. G. Nocera, *Proc. Natl. Acad. Sci. U. S. A.*, 2006, **103**, 15729–15735.
6 R. van de Krol and M. Grätzel, in *Photoelectrochemical Hydrogen Production*, ed. R. van de Krol and M. Grätzel, Springer, US, 2012, DOI: 10.1007/978-1-4614-1380-6.
7 M. Romero and A. Steinfeld, *Energy Environ. Sci.*, 2012, **5**, 9234–9245.
8 M. S. Whittingham, *Chem. Rev.*, 2004, **104**, 4271–4302.
9 U. S. G. Survey, https://www.usgs.gov/, 2017.
10 J. R. Scheffe and A. Steinfeld, *Mater. Today*, 2014, **17**, 341–348.
11 G. Centi, E. A. Quadrelli and S. Perathoner, *Energy Environ. Sci.*, 2013, **6**, 1711–1731.
12 C. Agrafiotis, M. Roeb and C. Sattler, *Renewable Sustainable Energy Rev.*, 2015, **42**, 254–285.
13 G. P. Smestad and A. Steinfeld, *Ind. Eng. Chem. Res.*, 2012, **51**, 11828–11840.
14 A. Steinfeld, *Sol. Energy*, 2005, **78**, 603–615.
15 C. Perkins and A. W. Weimer, *AIChE J.*, 2009, **55**, 286–293.
16 S. Abanades, P. Charvin, G. Flamant and P. Neveu, *Energy*, 2006, **31**, 2469–2486.
17 J. E. Miller, M. D. Allendorf, R. B. Diver, L. R. Evans, N. P. Siegel and J. N. Stuecker, *J. Mater. Sci.*, 2008, **43**, 4714–4728.
18 J. E. Funk, *Int. J. Hydrogen Energy*, 2001, **26**, 185–190.
19 T. Kodama and N. Gokon, *Chem. Rev.*, 2007, **107**, 4048–4077.
20 N. P. Siegel, J. E. Miller, I. Ermanoski, R. B. Diver and E. B. Stechel, *Ind. Eng. Chem. Res.*, 2013, **52**, 3276–3286.
21 J. Kim, T. A. Johnson, J. E. Miller, E. B. Stechel and C. T. Maravelias, *Energy Environ. Sci.*, 2012, **5**, 8417–8429.
22 G. J. Kolb and R. B. Diver, *Sandia Report 2008-1900*, 2008.
23 A. J. Traynor and R. J. Jensen, *Ind. Eng. Chem. Res.*, 2002, **41**, 1935–1939.
24 A. H. Bork, M. Kubicek, M. Struzik and J. L. M. Rupp, *J. Mater. Chem. A*, 2015, **3**, 15546–15557.
25 C. Perkins and A. W. Weimer, *Int. J. Hydrogen Energy*, 2004, **29**, 1587–1599.
26 T. Kodama, *Prog. Energy Combust. Sci.*, 2003, **29**, 567–597.
27 E. Bilgen, M. Ducarroir, M. Foex, F. Sibieude and F. Trombe, *Int. J. Hydrogen Energy*, 1977, **2**, 251–257.
28 H. Kaneko, N. Gokon, N. Hasegawa and Y. Tamaura, *Energy*, 2005, **30**, 2171–2178.
29 Y. Tamaura, A. Steinfeld, P. Kuhn and K. Ehrensberger, *Energy*, 1995, **20**, 325–330.
30 T. Nakamura, *Sol. Energy*, 1977, **19**, 467–475.
31 R. B. Diver, J. E. Miller, M. D. Allendorf, N. P. Siegel and R. E. Hogan, *Trans. ASME: J. Sol. Energy Eng.*, 2008, **130**, 0410011–0410018.
32 T. Kodama, Y. Nakamuro and T. Mizuno, *Trans. ASME: J. Sol. Energy Eng.*, 2006, **128**, 3–7.
33 M. D. Allendorf, R. B. Diver, N. P. Siegel and J. E. Miller, *Energy Fuels*, 2008, **22**, 4115–4124.
34 C. Perkins, P. R. Lichty and A. W. Weimer, *Int. J. Hydrogen Energy*, 2008, **33**, 499–510.
35 A. Steinfeld, *Int. J. Hydrogen Energy*, 2002, **27**, 611–619.
36 W. Villasmil, M. Brkic, D. Wuillemin, A. Meier and A. Steinfeld, *Trans. ASME: J. Sol. Energy Eng.*, 2014, **136**, 011017.

37 E. Koepf, W. Villasmil and A. Meier, *Appl. Energy*, 2016, **165**, 1004–1023.
38 W. C. Chueh, C. Falter, M. Abbott, D. Scipio, P. Furler, S. M. Haile and A. Steinfeld, *Science*, 2010, **330**, 1797–1801.
39 W. C. Chueh and S. M. Haile, *Philos. Trans. R. Soc., A*, 2010, **368**, 3269–3294.
40 W. C. Chueh and S. M. Haile, *ChemSusChem*, 2009, **2**, 735–739.
41 M. Kang, X. Wu, J. Zhang, N. Zhao, W. Wei and Y. Sun, *RSC Adv.*, 2014, **4**, 5583–5590.
42 J. R. Scheffe, R. Jacot, G. R. Patzke and A. Steinfeld, *J. Phys. Chem. C*, 2013, **117**, 24104–24110.
43 M. Takacs, J. R. Scheffe and A. Steinfeld, *Phys. Chem. Chem. Phys.*, 2015, **17**, 7813–7822.
44 H. Kaneko, H. Ishihara, S. Taku, Y. Naganuma, N. Hasegawa and Y. Tamaura, *J. Mater. Sci.*, 2008, **43**, 3153–3161.
45 H. Kaneko, T. Miura, H. Ishihara, S. Taku, T. Yokoyama, H. Nakajima and Y. Tamaura, *Energy*, 2007, **32**, 656–663.
46 P. Furler, J. Scheffe, D. Marxer, M. Gorbar, A. Bonk, U. Vogt and A. Steinfeld, *Phys. Chem. Chem. Phys.*, 2014, **16**, 10503–10511.
47 C. D. Malonzo, R. M. De Smith, S. G. Rudisill, N. D. Petkovich, J. H. Davidson and A. Stein, *J. Phys. Chem. C*, 2014, **118**, 26172–26181.
48 P. Furler, J. R. Scheffe and A. Steinfeld, *Energy Environ. Sci.*, 2012, **5**, 6098–6103.
49 J. R. Scheffe, M. Welte and A. Steinfeld, *Ind. Eng. Chem. Res.*, 2014, **53**, 2175–2182.
50 D. Marxer, P. Furler, J. Scheffe, H. Geerlings, C. Falter, V. Batteiger, A. Sizmann and A. Steinfeld, *Energy Fuels*, 2015, **29**, 3241–3250.
51 J. B. Goodenough, *Rep. Prog. Phys.*, 2004, **67**, 1915–1993.
52 M. A. Peña and J. L. G. Fierro, *Chem. Rev.*, 2001, **101**, 1981–2017.
53 S. Stølen, E. Bakken and C. E. Mohn, *Phys. Chem. Chem. Phys.*, 2006, **8**, 429–447.
54 A. S. Bhalla, R. Guo and R. Roy, *Mater. Res. Innovations*, 2000, **4**, 3–26.
55 J. Richter, P. Holtappels, T. Graule, T. Nakamura and L. J. Gauckler, *Monatsh. Chem.*, 2009, **140**, 985–999.
56 C. K. Yang, Y. Yamazaki, A. Aydin and S. M. Haile, *J. Mater. Chem. A*, 2014, **2**, 13612–13623.
57 A. Demont and S. Abanades, *RSC Adv.*, 2014, **4**, 54885–54891.
58 J. R. Scheffe, D. Weibel and A. Steinfeld, *Energy Fuels*, 2013, **27**, 4250–4257.
59 A. Evdou, V. Zaspalis and L. Nalbandian, *Int. J. Hydrogen Energy*, 2008, **33**, 5554–5562.
60 L. Nalbandian, A. Evdou and V. Zaspalis, *Int. J. Hydrogen Energy*, 2009, **34**, 7162–7172.
61 S. Dey, B. S. Naidu and C. N. R. Rao, *Chem.–Eur. J.*, 2015, **21**, 7077–7081.
62 S. Dey, B. S. Naidu, A. Govindaraj and C. N. R. Rao, *Phys. Chem. Chem. Phys.*, 2015, **17**, 122–125.
63 A. M. Deml, V. Stevanović, A. M. Holder, M. Sanders, R. Ohayre and C. B. Musgrave, *Chem. Mater.*, 2014, **26**, 6595–6602.
64 A. H. McDaniel, E. C. Miller, D. Arifin, A. Ambrosini, E. N. Coker, R. O'Hayre, W. C. Chueh and J. Tong, *Energy Environ. Sci.*, 2013, **6**, 2424–2428.
65 A. Demont and S. Abanades, *J. Mater. Chem. A*, 2015, **3**, 3536–3546.
66 M. E. Gálvez, R. Jacot, J. Scheffe, T. Cooper, G. Patzke and A. Steinfeld, *Phys. Chem. Chem. Phys.*, 2015, **17**, 6629–6634.
67 A. Demont, S. Abanades and E. Beche, *J. Phys. Chem. C*, 2014, **118**, 12682–12692.
68 M. Takacs, M. Hoes, M. Caduff, T. Cooper, J. R. Scheffe and A. Steinfeld, *Acta Mater.*, 2016, **103**, 700–710.
69 D. Yadav and R. Banerjee, *Renewable Sustainable Energy Rev.*, 2016, **54**, 497–532.
70 S. A. M. Said, M. Waseeuddin and D. S. A. Simakov, *Renewable Sustainable Energy Rev.*, 2016, **59**, 149–159.
71 P. J. Valades-Pelayo, H. Romero-Paredes, C. A. Arancibia-Bulnes and H. I. Villafán-Vidales, *Appl. Therm. Eng.*, 2016, **98**, 575–581.
72 L. J. Venstrom, R. M. De Smith, R. Bala Chandran, D. B. Boman, P. T. Krenzke and J. H. Davidson, *Energy Fuels*, 2015, **29**, 8168–8177.
73 A. Steinfeld, M. Brack, A. Meier, A. Weidenkaff and D. Wuillemin, *Energy*, 1998, **23**, 803–814.
74 A. Weidenkaff, M. Brack, S. Möller, R. Palumbo and A. Steinfeld, *J. Phys. IV*, 1999, **9**, Pr3-313.
75 I. Ermanoski, N. P. Siegel and E. B. Stechel, *J. Sol. Energy Eng.*, 2013, **135**, 031002.
76 A. Z'Graggen, P. Haueter, G. Maag, A. Vidal, M. Romero and A. Steinfeld, *Int. J. Hydrogen Energy*, 2007, **32**, 992–996.
77 A. Z'Graggen and A. Steinfeld, *Int. J. Hydrogen Energy*, 2008, **33**, 5484–5492.
78 N. Piatkowski and A. Steinfeld, *AIChE J.*, 2011, **57**, 3522–3533.
79 C. Yuan, C. Jarrett, W. Chueh, Y. Kawajiri and A. Henry, *Sol. Energy*, 2015, **122**, 547–561.
80 D. Marxer, P. Furler, M. Takacs and A. Steinfeld, *Energy Environ. Sci.*, 2017, **10**, 1142–1149.
81 R. E. Schaak and T. E. Mallouk, *Chem. Mater.*, 2002, **14**, 1455–1471.
82 J. H. Kim and A. Manthiram, *J. Electrochem. Soc.*, 2008, **155**, B385–B390.
83 C. J. Howard, B. J. Kennedy and P. M. Woodward, *Acta Crystallogr., Sect. B: Struct. Sci.*, 2003, **59**, 463–471.
84 H. J. Snaith, *J. Phys. Chem. Lett.*, 2013, **4**, 3623–3630.
85 B. V. Lotsch, *Angew. Chem., Int. Ed.*, 2014, **53**, 635–637.
86 M. Y. Chern, D. A. Vennos and F. J. Disalvo, *J. Solid State Chem.*, 1992, **96**, 415–425.
87 Y. Zhao and L. L. Daemen, *J. Am. Chem. Soc.*, 2012, **134**, 15042–15047.
88 V. M. Goldschmidt, *Naturwissenschaften*, 1926, **14**, 477–485.
89 D. S. Aidhy and W. J. Weber, *J. Mater. Res.*, 2016, **31**, 2–16.
90 S. T. Murphy, E. E. Jay and R. W. Grimes, *J. Nucl. Mater.*, 2014, **447**, 143–149.

91 R. J. D. Tilley, in *Defects in Solids*, John Wiley & Sons, Inc., 2008, pp. 83–133, DOI: 10.1002/9780470380758.ch3.
92 J. Mizusaki, N. Mori, H. Takai, Y. Yonemura, H. Minamiue, H. Tagawa, M. Dokiya, H. Inaba, K. Naraya, T. Sasamoto and T. Hashimoto, *Solid State Ionics*, 2000, **129**, 163–177.
93 J. A. M. Van Roosmalen, E. H. P. Cordfunke, R. B. Helmholdt and H. W. Zandbergen, *J. Solid State Chem.*, 1994, **110**, 100–105.
94 R. A. De Souza, M. S. Islam and E. Ivers-Tiffée, *J. Mater. Chem.*, 1999, **9**, 1621–1627.
95 A. Jones and M. S. Islam, *J. Phys. Chem. C*, 2008, **112**, 4455–4462.
96 R. A. De Souza and J. Maier, *Phys. Chem. Chem. Phys.*, 2003, **5**, 740–748.
97 P. D. Battle, J. E. Bennett, J. Sloan, R. J. D. Tilley and J. F. Vente, *J. Solid State Chem.*, 2000, **149**, 360–369.
98 M. Abe and K. Uchino, *Mater. Res. Bull.*, 1974, **9**, 147–155.
99 J. Ovenstone, J. S. White and S. T. Misture, *J. Power Sources*, 2008, **181**, 56–61.
100 V. Caignaert, N. Nguyen, M. Hervieu and B. Raveau, *Mater. Res. Bull.*, 1985, **20**, 479–484.
101 J. A. Alonso, M. J. Martínez-Lope, J. L. García-Muñoz and M. T. Fernández-Díaz, *J. Phys.: Condens. Matter*, 1997, **9**, 6417–6426.
102 L. Er-Rakho, C. Michel and B. Raveau, *J. Solid State Chem.*, 1988, **73**, 514–519.
103 Z. Shao and S. M. Halle, *Nature*, 2004, **431**, 170–173.
104 A. S. Harvey, F. J. Litterst, Z. Yang, J. L. M. Rupp, A. Infortuna and L. J. Gauckler, *Phys. Chem. Chem. Phys.*, 2009, **11**, 3090–3098.
105 S. McIntosh, J. F. Vente, W. G. Haije, D. H. A. Blank and H. J. M. Bouwmeester, *Chem. Mater.*, 2006, **18**, 2187–2193.
106 S. Švarcová, K. Wiik, J. Tolchard, H. J. M. Bouwmeester and T. Grande, *Solid State Ionics*, 2008, **178**, 1787–1791.
107 J. Ovenstone, J. I. Jung, J. S. White, D. D. Edwards and S. T. Misture, *J. Solid State Chem.*, 2008, **181**, 576–586.
108 R. J. Panlener, R. N. Blumenthal and J. E. Garnier, *J. Phys. Chem. Solids*, 1975, **36**, 1213–1222.
109 R. Shannon, *Acta Crystallogr., Sect. A: Cryst. Phys., Diffr., Theor. Gen. Crystallogr.*, 1976, **32**, 751–767.
110 *SpringerMaterials*, ed. O. Madelung, U. Rössler and M. Schulz, Springer-Verlag, Berlin Heidelberg, 2000, DOI: 10.1007/10717201_1101.
111 A. Urushibara, Y. Moritomo, T. Arima, A. Asamitsu, G. Kido and Y. Tokura, *Phys. Rev. B: Condens. Matter Mater. Phys.*, 1995, **51**, 14103–14109.
112 J. M. D. Coey, M. Viret and S. Von Molnár, *Adv. Phys.*, 1999, **48**, 167–293.
113 F. A. Kröger and H. J. Vink, in *Solid State Physics*, ed. S. Frederick and T. David, Academic Press, 1956, vol. 3, pp. 307–435.
114 B. Meredig and C. Wolverton, *Phys. Rev. B: Condens. Matter Mater. Phys.*, 2009, **80**, 245119.
115 J. E. Miller, A. H. McDaniel and M. D. Allendorf, *Adv. Energy Mater.*, 2014, **4**, 1300469.
116 J. R. Scheffe and A. Steinfeld, *Energy Fuels*, 2012, **26**, 1928–1936.
117 S. Onuma, K. Yashiro, S. Miyoshi, A. Kaimai, H. Matsumoto, Y. Nigara, T. Kawada, J. Mizusaki, K. Kawamura and N. Sakai, *Solid State Ionics*, 2004, **174**, 287–293.
118 J. Mizusaki, S. Yamauchi, K. Fueki and A. Ishikawa, *Solid State Ionics*, 1984, **12**, 119–124.
119 J. Mizusaki, H. Tagawa, K. Naraya and T. Sasamoto, *Solid State Ionics*, 1991, **49**, 111–118.
120 M. Oishi, K. Yashiro, K. Sato, J. Mizusaki and T. Kawada, *J. Solid State Chem.*, 2008, **181**, 3177–3184.
121 T. Cooper, J. R. Scheffe, M. E. Galvez, R. Jacot, G. Patzke and A. Steinfeld, *Energy Technol.*, 2015, **3**, 1130–1142.
122 J. Mizusaki, M. Yoshihiro, S. Yamauchi and K. Fueki, *J. Solid State Chem.*, 1985, **58**, 257–266.
123 M. Kuhn, Y. Fukuda, S. Hashimoto, K. Sato, K. Yashiro and J. Mizusaki, *J. Electrochem. Soc.*, 2013, **160**, F34–F42.
124 J. Mizusaki, Y. Mima, S. Yamauchi, K. Fueki and H. Tagawa, *J. Solid State Chem.*, 1989, **80**, 102–111.
125 A. H. McDaniel, E. C. Miller, D. Arifin, A. Ambrosini, E. N. Coker, R. O'Hayre, W. C. Chueh and J. Tong, *Energy Environ. Sci.*, 2013, **6**, 2424–2428.
126 J. R. Scheffe, D. Weibel and A. Steinfeld, *Energy Fuels*, 2013, **27**, 4250–4257.
127 M. Takacs, M. Hoes, M. Caduff, T. Cooper, J. Scheffe and A. Steinfeld, *Acta Mater.*, 2016, **103**, 700–710.
128 H. L. Lukas, S. G. Fries and B. Sundman, *Computational thermodynamics: the Calphad method*, Cambridge university press Cambridge, 2007.
129 L. Kaufman and H. Bernstein, 1970.
130 Z.-K. Liu, *J. Phase Equilib. Diffus.*, 2009, **30**, 517–534.
131 A. H. Bork, E. Povoden-Karadeniz and J. L. M. Rupp, *Adv. Energy Mater.*, 2017, **7**, 1601086.
132 A. N. Grundy, B. Hallstedt and L. J. Gauckler, *Acta Mater.*, 2002, **50**, 2209–2222.
133 A. N. Grundy, B. Hallstedt and L. J. Gauckler, *J. Phase Equilib. Diffus.*, 2004, **25**, 311–319.
134 E. Povoden, M. Chen, A. Grundy, T. Ivas and L. Gauckler, *J. Phase Equilib. Diffus.*, 2009, **30**, 12–27.
135 E. Povoden-Karadeniz, M. Chen, T. Ivas, A. Grundy and L. Gauckler, *J. Mater. Res.*, 2012, **27**, 1915–1926.
136 A. A. Emery, J. E. Saal, S. Kirklin, V. I. Hegde and C. Wolverton, *Chem. Mater.*, 2016, **28**, 5621–5634.
137 A. M. Deml, V. Stevanović, C. L. Muhich, C. B. Musgrave and R. O'Hayre, *Energy Environ. Sci.*, 2014, **7**, 1996–2004.
138 A. M. Deml, V. Stevanović, A. M. Holder, M. Sanders, R. O'Hayre and C. B. Musgrave, *Chem. Mater.*, 2014, **26**, 6595–6602.
139 R. Michalsky, V. Botu, C. M. Hargus, A. A. Peterson and A. Steinfeld, *Adv. Energy Mater.*, 2015, **5**, 1401082-n/a.
140 J. C. Ruiz-Morales, D. Marrero-López, J. Canales-Vázquez and J. T. S. Irvine, *RSC Adv.*, 2011, **1**, 1403–1414.
141 M. Ni, M. K. H. Leung and D. Y. C. Leung, *Int. J. Hydrogen Energy*, 2008, **33**, 2337–2354.
142 L. Bi, S. Boulfrad and E. Traversa, *Chem. Soc. Rev.*, 2014, **43**, 8255–8270.
143 S. B. Adler, *Chem. Rev.*, 2004, **104**, 4791–4843.

144 R. Merkle and J. Maier, *Phys. Chem. Chem. Phys.*, 2002, **4**, 4140–4148.
145 K. Zheng, A. Klimkowicz, K. Świerczek, A. Malik, Y. Ariga, T. Tominaga and A. Takasaki, *J. Alloys Compd.*, 2015, **645**, S357–S360.
146 W. Preis, E. Bucher and W. Sitte, *Solid State Ionics*, 2004, **175**, 393–397.
147 M. Søgaard, A. Bieberle-Hütter, P. V. Hendriksen, M. Mogensen and H. L. Tuller, *J. Electroceram.*, 2011, **27**, 134–142.
148 E. Bucher, C. Gspan, F. Hofer and W. Sitte, *Solid State Ionics*, 2013, **238**, 15–23.
149 A. Falkenstein, D. N. Mueller, R. A. De Souza and M. Martin, *Solid State Ionics*, 2015, **280**, 66–73.
150 R. Hancke, S. Fearn, J. A. Kilner and R. Haugsrud, *Phys. Chem. Chem. Phys.*, 2012, **14**, 13971–13978.
151 J. Maier, *Physical Chemistry of Ionic Materials. Ions and Electrons in Solids*, John Wiley & Sons, Ltd, Chichester, 2004.
152 C. Tregambi, R. Chirone, F. Montagnaro, P. Salatino and R. Solimene, *Sol. Energy*, 2016, **129**, 85–100.
153 P. Pozivil, S. Ackermann and A. Steinfeld, *Trans. ASME: J. Sol. Energy Eng.*, 2015, **137**, 064504.
154 L. S. Walker, J. E. Miller, G. E. Hilmas, L. R. Evans and E. L. Corral, *Energy Fuels*, 2012, **26**, 712–721.
155 P. Furler, J. Scheffe, M. Gorbar, L. Moes, U. Vogt and A. Steinfeld, *Energy Fuels*, 2012, **26**, 7051–7059.
156 A. Steinfeld, A. Frei, P. Kuhn and D. Wuillemin, *Int. J. Hydrogen Energy*, 1995, **20**, 793–804.
157 G. Flamant, D. Gauthier, C. Boudhari and Y. Flitris, *Trans. ASME: J. Sol. Energy Eng.*, 1988, **110**, 313–320.
158 A. Meier, J. Ganz and A. Steinfeld, *Chem. Eng. Sci.*, 1996, **51**, 3181–3186.
159 N. Gokon, S. Takahashi, H. Yamamoto and T. Kodama, *Int. J. Hydrogen Energy*, 2008, **33**, 2189–2199.
160 E. Alonso and M. Romero, *Renewable Sustainable Energy Rev.*, 2015, **41**, 53–67.
161 G. Joaquín, M. C. Sánchez, S. Gloria and B. Javier, *J. Phys.: Condens. Matter*, 2001, **13**, 3229.
162 O. Toulemonde, F. Studer, A. Barnabé, A. Maignan, C. Martin and B. Raveau, *Eur. Phys. J. B*, 1998, **4**, 159–167.
163 M. Sikora, C. Kapusta, K. Knížek, Z. Jirák, C. Autret, M. Borowiec, C. J. Oates, V. Procházka, D. Rybicki and D. Zajac, *Phys. Rev. B: Condens. Matter Mater. Phys.*, 2006, **73**, 094426.
164 G. Saracco, F. Geobaldo and G. Baldi, *Appl. Catal., B*, 1999, **20**, 277–288.
165 R. Le Toquin, W. Paulus, A. Cousson, C. Prestipino and C. Lamberti, *J. Am. Chem. Soc.*, 2006, **128**, 13161–13174.
166 A. Piovano, G. Agostini, A. I. Frenkel, T. Bertier, C. Prestipino, M. Ceretti, W. Paulus and C. Lamberti, *J. Phys. Chem. C*, 2011, **115**, 1311–1322.
167 A. K. Huber, M. Falk, M. Rohnke, B. Luerßen, L. Gregoratti, M. Amati and J. Janek, *Phys. Chem. Chem. Phys.*, 2012, **14**, 751–758.
168 E. J. Crumlin, E. Mutoro, W. T. Hong, M. D. Biegalski, H. M. Christen, Z. Liu, H. Bluhm and Y. Shao-Horn, *J. Phys. Chem. C*, 2013, **117**, 16087–16094.
169 A. K. Opitz, A. Nenning, C. Rameshan, R. Rameshan, R. Blume, M. Hävecker, A. Knop-Gericke, G. Rupprechter, J. Fleig and B. Klötzer, *Angew. Chem., Int. Ed.*, 2015, **54**, 2628–2632.
170 W. H. Weber and R. Merlin, *Raman scattering in materials science*, Springer Science & Business Media, 2013.
171 M. N. Iliev and M. V. Abrashev, *J. Raman Spectrosc.*, 2001, **32**, 805–811.
172 M. Abrashev, A. Litvinchuk, M. Iliev, R. Meng, V. Popov, V. Ivanov, R. Chakalov and C. Thomsen, *Phys. Rev. B: Condens. Matter Mater. Phys.*, 1999, **59**, 4146.
173 E. Granado, A. Garcia, J. Sanjurjo, C. Rettori, I. Torriani, F. Prado, R. Sanchez, A. Caneiro and S. Oseroff, *Phys. Rev. B: Condens. Matter Mater. Phys.*, 1999, **60**, 11879.
174 V. Podobedov, A. Weber, D. Romero, J. Rice and H. Drew, *Phys. Rev. B: Condens. Matter Mater. Phys.*, 1998, **58**, 43.
175 A. De Andrés, J. Martínez, J. Alonso, E. Herrero, C. Prieto, J. Alonso, F. Agullo and M. Garcia-Hernández, *J. Magn. Magn. Mater.*, 1999, **196**, 453–454.
176 M. Popa, J. Frantti and M. Kakihana, *Solid State Ionics*, 2002, **154**, 135–141.
177 E. Traversa, P. Nunziante, L. Sangaletti, B. Allieri, L. E. Depero, H. Aono and Y. Sadaoka, *J. Am. Ceram. Soc.*, 2000, **83**, 1087–1092.
178 S. Ackermann, L. Sauvin, R. Castiglioni, J. L. Rupp, J. R. Scheffe and A. Steinfeld, *J. Phys. Chem. C*, 2015, **119**, 16452–16461.
179 C.-K. Yang, Y. Yamazaki, A. Aydin and S. M. Haile, *J. Mater. Chem. A*, 2014, **2**, 13612–13623.
180 I. Ermanoski, J. Miller and M. Allendorf, *Phys. Chem. Chem. Phys.*, 2014, **16**, 8418–8427.
181 N. P. Siegel, J. E. Miller, I. Ermanoski, R. B. Diver and E. B. Stechel, *Ind. Eng. Chem. Res.*, 2013, **52**, 3276–3286.
182 M. Takacs, J. Scheffe and A. Steinfeld, *Phys. Chem. Chem. Phys.*, 2015, **17**, 7813–7822.
183 C. Jarrett, W. Chueh, C. Yuan, Y. Kawajiri, K. H. Sandhage and A. Henry, *Sol. Energy*, 2016, **123**, 57–73.